DETERMINATION OF LOCAL MOVEMENTS OF THE FG-LOOP AND ALPHA-HELIX OF SODIUM-CALCIUM EXCHANGER NCX1.1 UPON BINDING OF CALCIUM IONS USING EPR

By

Gage Franklin Matthews

Thesis

Submitted to the Faculty of the

Graduate School of Vanderbilt University

In partial fulfillment of requirements

for the degree of

MASTER OF SCIENCE

in

Chemical and Physical Biology

August, 2012

Nashville, Tennessee

Accepted:

Professor Albert Beth

Professor Hassane Mchaourab

Professor Chuck Sanders

To my parents, who unceasingly support me through all that I do.

To Krissa, Marcus, and Silas for giving me something to look forward to throughout this process.

To Katelyn for her undying encouragement and belief in me.

ACKNOWLEDGMENTS

I would like to thank everyone that I have encountered at Vanderbilt for providing a nurturing, comfortable environment for my studies. Dr. Chuck Sanders was a driving force in my interest in coming to Vanderbilt, and I would be remiss to not thank him for helping me find this opportunity. Without his seminar at St. Olaf and following conversation, I would not be where I am today. Dr. Hassane Mchaourab was always willing to discuss anything I needed, and I am indescribably indebted to him for his guidance. I would also like to thank my co-students in the CPB program, who have given me many laughs and many chances to commiserate. Lindsay Meyers has also given me innumerable opportunities to be involved with the interview process of visiting applicants, which was always one of my favorite times of the year.

Of course, all of this would not be possible without the mentorship of Dr. Al Beth, who was consistently encouraging and happy to have me working on this project. His funding of this project paved the way for my work and his advice was always welcome, and he was an important source of guidance for this research. Dr. Neena Dixit and Dr. Sunghoon Kim were also invaluable for their help as I learned the ropes of protein preparation and EPR, respectively. Suzanne Brandon and Dr. Eric Hustedt also provided necessary assistance at points when I needed it most. I also have to thank Dr. Walter Chazin and the Molecular Biophysics Training Program for funding and support along the way.

Finally, I have to acknowledge my parents, whose undying support throughout my life continues to amaze me. Without their guidance in all walks of life, I would be

lost. My sister Krissa and brother Marcus always provided some fun family interactions to look forward to, and their son Silas has given me a bright spot to think of everyday. Katelyn has always motivated me and helped me find the best path for me, and her determined support of my decisions has been exceedingly important for me.

TABLE OF CONTENTS

Page

List of Figures

Figure Page

CHAPTER I

INTRODUCTION

Rationale for Dissertation

All mammalian cells rely on ions for any number of biological tasks and processes. These can be a number of various ions, but the transport of them into, out of, and within each cell is exceedingly important. In the heart, for instance, transport of calcium ions into and out of cardiomyocytes' cytoplasm is one of the main control mechanisms for contraction and relaxation during heart beats. Multiple ion transporters are needed for this process, but the sodium-calcium exchanger NCX1.1 is of particular interest. NCX1.1 is one of 17 isoforms of the gene for NCX1 and exists in a superfamily of sodium-calcium and sodium-potassium exchangers, many of which share structural or sequence similarities with NCX1.1. While issues with NCX1.1 can be involved with heart failure, mutations, loss of expression, or other problems, the other superfamily members can be involved in a wide variety of diseases, including Alzheimer's Disease, epilepsy, Andersen-Tawil Syndrom, and Long QT Syndrome, among others. These examples strongly exhibit the necessity of such transporters for normal cell survival.

While it is well-known that these proteins, including NCX1.1, are vitally important, structural details of the exchange mechanism have been more difficult to come by. X-ray crystallography, nuclear magnetic resonance (NMR) spectroscopy, small-angle x-ray spectroscopy (SAXS), and Fórster resonance energy transfer (FRET) have all been used to understand some facets of the structure and/or mechanism of activity. Information

from these techniques has allowed for further research using electron paramagnetic resonance (EPR) to hone in on specific movements and components of the exchange mechanism.

Previous work has shown that the FG-loop of NCX1.1, or the site of splice variation in NCX1 isoforms, is important for normal activity. This FG-loop includes a small α-helix and has been seen as an unstructured region in previous structures determined by NMR. This dissertation uses EPR techniques with side-directed spin labeling (SDSL) to investigate the movements of this region upon calcium binding. Because of the necessity of the FG-loop and α-helix – and the similarity of the structure to other exchangers – these findings can be useful for understanding how a wide variety of exchanger proteins are able to transport their ions and what structural steps are involved in carrying out that process.

Systole and Diastole in Cardiomyocytes

Blood circulation in mammals is critical for their survival, and the mechanism of pumping this blood throughout the body is therefore of great interest. Mammals, like other organisms, use muscular hearts to propel blood through their bodies, carrying oxygen to all cells by way of a vascular network of interconnecting arteries, veins, and capillaries. This movement requires specific activity from the cardiomyocytes which compose the majority of cardiac tissue. The activity of cardiomyocytes falls into a cycle of systole and diastole that is governed by the action potential of those cells (Hill et al. 2008).

During systole, the ventricles of the heart contract, which raises the pressure of the fixed amount of blood they hold until the aortic valves open to allow blood to flow to the aorta and on to the body (Hill et al. 2008). Although each ventricle pumps blood in a different direction – the right ventricle pumps unoxygenated blood to the lungs, while the left ventricle pumps oxygenated blood through the circulatory system – the pumping process happens concurrently. Once most of the blood is ejected from the ventricles, the ventricles relax, signaling the start of diastole. As the pressure in the atria exceeds that in the ventricles, the aortic valves close to cut off unwanted blood flow and the ventricles refill with blood via the atrioventricular valves. This cyclical system continues as unoxygenated blood is saturated with oxygen in the lungs and sent through the left ventricle to the body, returning deoxygenated blood to the right ventricle and, thus, restarting the cycle (Hill et al. 2008).

Each large motion of the heart and ventricles is controlled by much smaller movements in the muscle cells of the heart: cardiomyocytes. These cells are responsible for the contraction and relaxation of the ventricles, a necessity for normal heart performance. As with all myocytes, cardiomyocytes rely on their cellular skeleton for their function. Each long cell contains many branching myofibrils, each roughly 10-20 Å in diameter (Alberts et al. 2007). These myofibrils are built from repeats of sarcomeres, which are complexes of overlapping filamentous proteins used for muscle contraction. These filamentous proteins include myosin, actin, nebulin, titin, tropomodulin, tropomyosin, and troponin, among other proteins that associate during the process of contraction and relaxation. The structure of their interactions can be seen in Figure 1.

Unique versions of these proteins are present in cardiomyocytes to accommodate the heavier workload of the heart (Alberts et al. 2007).

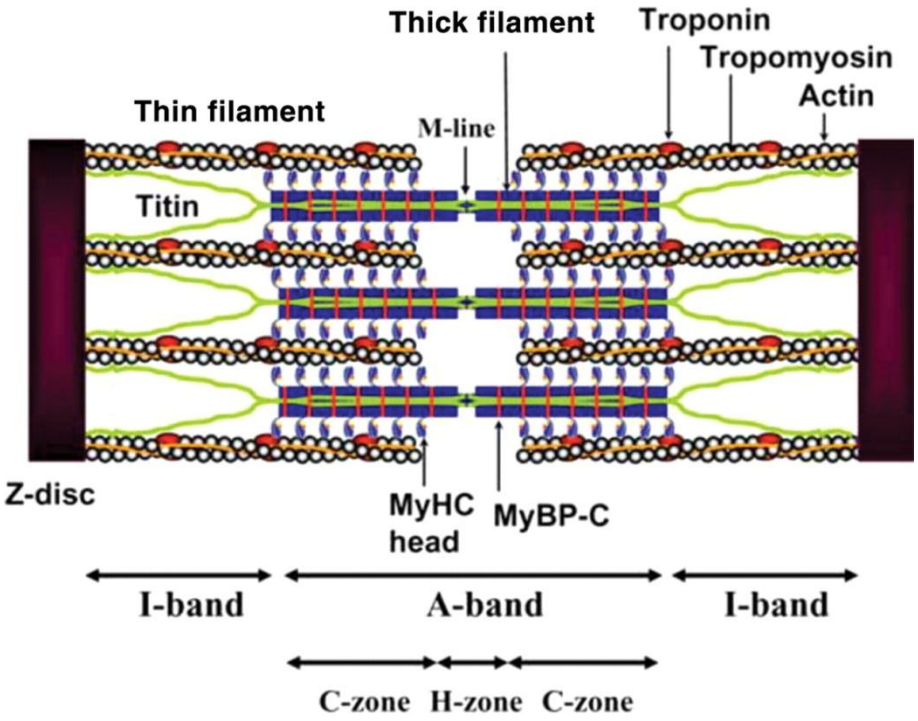

FIGURE 1. The structure of a sarcomere in different states, from contraction to over-extension. This shows the arrangement of the components of a sarcomere. During muscle contraction, the myosin molecules (My) will "walk" along actin toward the Z-discs on either side, pulling those Z-discs together and contracting the muscle. (Figure from Morimoto 2007)

At the molecular level, an incoming action potential, generated in the heart, triggers an influx of calcium ions. The initial ions come from across the cell membrane by way of the L-type calcium channel, a voltage-gated channel that responds to membrane depolarization during diastole (López-López et al. 1995). Because these channels cannot import a large enough quantity of calcium ions to cause a quick contraction of the heart, other sources, like the sarcoplasmic reticulum (SR), are used to rapidly increase the cytosolic calcium concentration. Ion transporter proteins, like the

sodium-calcium exchanger (NCX) and especially the ryanodine receptor (RyR), are required to move the ions past the nonpolar tails of membrane phospholipids and into the cytosol. Roughly 80% of the calcium ions in this process are transported out of the SR via RyR, as opposed to the 20% imported by L-type calcium channels and NCX (Delbridge et al. 1996). The flow of ions and important enzymes for this process can be seen in Figure 2.

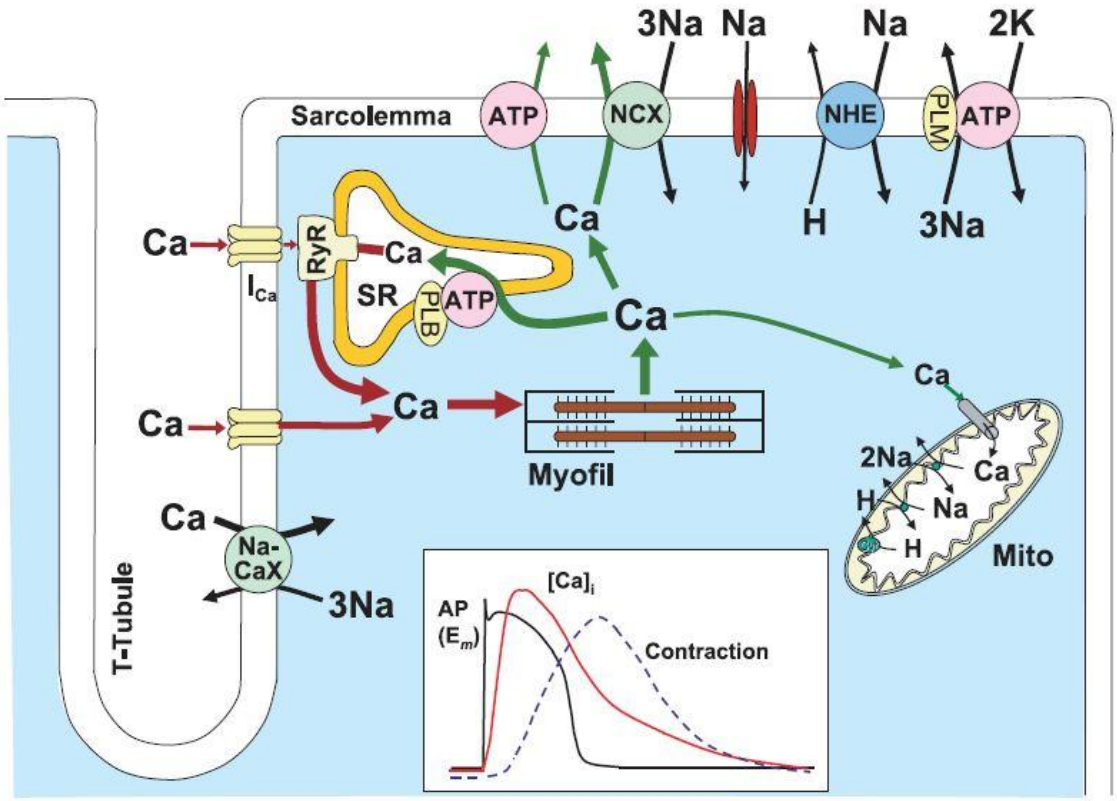

FIGURE 2. A diagram of the ion flow in a cardiomyocyte, feature the ryanodine receptor (RyR), sarcoendoplasmic reticulum ATPase (ATP in SR membrane), and sodium-calcium exchanger (Na-CaX or NCX). Inset shows the time course of an action potential, change in intracellular calcium concentration, and normal contraction course. (Bers and Despa 2006)

When the concentration of calcium ions in the cell rises, the protein complex troponin will bind up to four calcium molecules and release actin, causing tropomyosin to slide away from myosin binding sites. Myosin, an ATP-dependent motor protein, is then able to walk along actin and pull sarcomere ends, named Z-discs after the Cap Z protein that composes them, toward one another (Alberts et al. 2007). This movement is the ultimate contraction of the heart. Soon after the calcium ions are transported into the cytoplasm, the sarco-endoplasmic reticulum calcium ATPase (SERCA) pump starts hydrolyzing ATP to move these ions back into the SR (Periasamy and Huke 2001). This action causes troponin to release calcium ions and rebind actin, impeding myosin binding and relaxing the myofibril (Alberts et al. 2007). The high concentration of calcium ions also triggers calcium extrusion across the sarcolemma via NCX to increase the rate of relaxation (Hilgemann 1990). The frequent movement of ions into and out of the cytoplasm during contraction and relaxation highlights the necessity of ion transporters for normal cardiac function.

Ion Transport

The transport of ions across cell membranes is an extremely important facet of many cellular processes, including myofibril contraction. Without correct ion or charge gradients across the membrane, tasks such as muscle contraction or neural signaling are unable to occur (Gouaux and MacKinnon 2005). The effects of inadequate ion regulation are manifested throughout the body and often involve incorrect forms of ion-transporting proteins. When these issues arise, many diseases may develop, including cystic fibrosis and Bartter syndrome. Other effects may include abnormal insulin secretion, kidney

stones, and osteopetrosis (Hübner and Jentsch 2002). Though just a small selection, this list highlights the need for knowledge regarding the physiology, structures, and mechanisms of ion transporters so that such disorders and detrimental effects can be combated.

Cells typically employ several types of proteins to transfer ions. These proteins' mechanisms for ion movement can be any in a wide range of options. Some, like typical ion channels, may simply facilitate diffusion, while others may actively move the ions across the membrane (Gouaux and MacKinnon 2005). No matter the mechanism, these proteins maintain a critical role in the normal function of a cell for many reasons, from the aforementioned medical issues to the difficulties in transporting ions across the membrane. While it is true that ion regulation is necessary for cell survival, the necessity of proteins to perform this process stems from two factors: ion gradients and the impermeability of membrane bilayers. Many ions have to be moved against their gradients using active transport, while some move with the gradient using passive or gated transport. Since ions can be large and are always polar, passing the tightly-packed membrane and its hydrophobic center without assistance is nearly impossible (Gouaux and MacKinnon 2005). Therefore, expressing proteins to transport these ions is a crucial component of cell viability.

Because of the critical nature of ion transport, proteins that carry out this process are expressed in all cell types. However, they can involve a number of different methods to transport ions. Some, like the bacterial potassium transporter KcsA, passively transport ions by facilitating diffusion (Doyle et al. 1998). Others, such as the mammalian sodium-potassium ATPase, actively transport ions, using ATP or energy from the transport of

another ion in the process (Jorgensen et al. 2003). The remainder of the ion transporters generally fall into the category of gated channels, which require certain ligands or environmental factors to open their pathways, allowing ions to flow down their concentration gradient (Nelson and Cox 2004).

The protein NCX, for example, is an antiporter protein that transports sodium and calcium in opposite directions (Reeves et al. 1994). Though it is a reversible mechanism, NCX will always antiport ions, with calcium entering the cell as sodium is extruded or vice versa. As such, NCX is an active transporter, harnessing the energy from moving three sodium ions to carry a single calcium ion across the membrane (Reeves et al. 1994). It's this action that is crucial in cardiomyocytes, as calcium control during systole and diastole is an exceptionally imperative process.

The Sodium-Calcium Exchanger NCX

NCX Genetics and Expression

When grouped together, the gene families SLC8 and SLC24 form a superfamily of sodium-calcium antiporters (Quednau et al. 2004). NCX is a member of SLC8, which is composed only of the three mammalian NCX variants: NCX1, NCX2, and NCX3. All three fit into the category of cation/calcium exchangers, which are vital for many calcium-dependent pathways and processes and includes the entire SLC8/24 superfamily (Cai and Lytton 2004). The topology of these proteins is their uniting structural feature, and most are similar to the topology of NCX (Quednau et al. 2004), as seen in Figure 3. Each features two domains of transmembrane helices and a cytosolic loop that varies in

length depending on the protein. Most members also feature one alpha site on each transmembrane domain, α-1 and α-2, which are known to be highly conserved among related proteins. These sites form the ion-binding pocket for ion exchange (Schwarz and Benzer 1997).

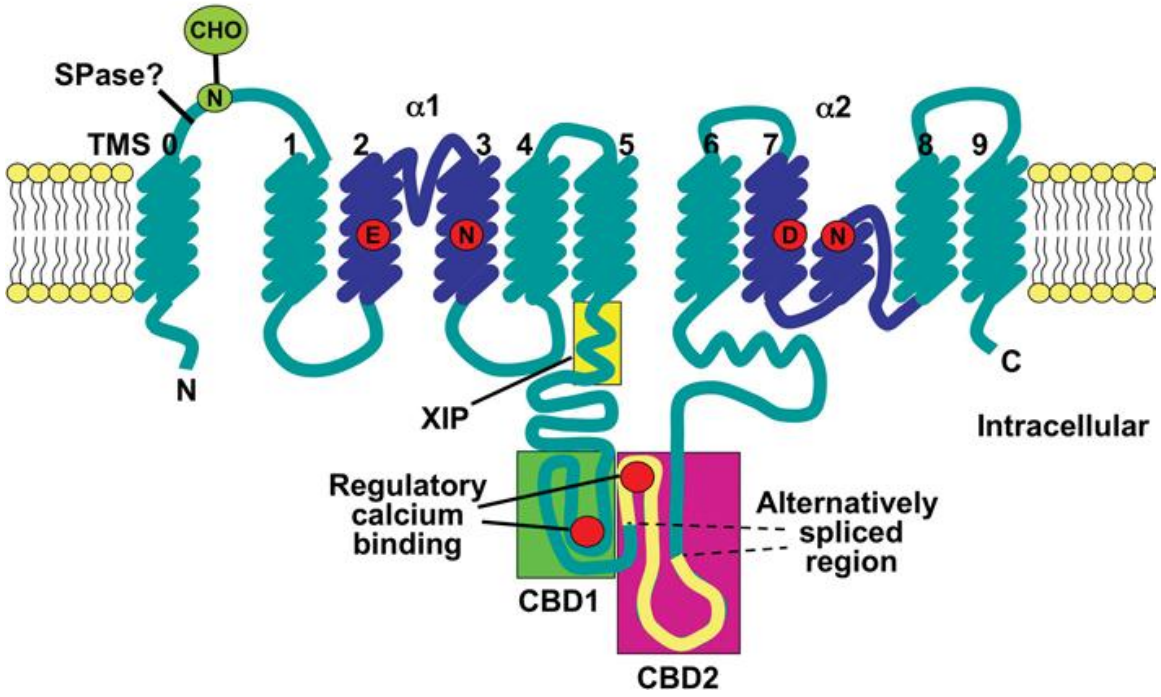

FIGURE 3. A topological model of NCX. Sites marked in red on the transmembrane helices are critical members of the α-sites. Dark blue transmembrane regions are locations of α-repeat motifs, as labeled. A site of N-linked glycosylation is shown in green. The alternatively spliced region of CBD2, which results in isoforms of each NCX gene, is also highlighted. (Lytton 2007)

The sodium-calcium exchanger, NCX, exists in nearly all cells of the mammalian body in various concentrations. However, each cell type or bodily region exhibits a different NCX protein, each of which is encoded in a different gene (Nicoll et al. 1990; Li et al. 1994; Nicoll et al. 1996). NCX1 is the most common isoform in the heart and kidneys, and is also highly expressed in the brain (Li et al. 1994). Conversely, high

NCX2 and NCX3 expression is restricted to neurons within the brain and skeletal muscle (Li et al. 1994; Nicoll et al. 1996). These three variants – NCX1, NCX2, and NCX3 – have roughly 70% amino acid sequence similarity (Quednau et al. 2004; Elbaz et al. 2008). The gene for each variant includes a region of small exons that can, in some cases, be spliced in various ways to produce tissue-specific isoforms. NCX2, for instance, produces no isoforms, while NCX3 can be spliced into very few (Quednau et al. 1997). Conversely, there are 17 NCX1 isoforms that each have different cell type specificities (Hilge et al. 2006). The isoform NCX1.1, for example, is the most prevalent in cardiomyocytes, while other types are expressed either at a low amount or not at all (Quednau et al. 1997). An example of this splicing is shown as NCX1.4 in Figure 4. The exact reasons for the differential expression are not yet clear, though physiological studies continue to explore the impacts each isoform can have in different environments. Previous research has shown that differential splicing changes the reactivity of NCX to calcium regulation, highlighting the necessity of understanding in this region (Breukels and Vuister 2010; Dyck et al. 1999). As these changes exist in different cell types and regions of the body, there may be significant implications of splicing for specific function in each variant's location.

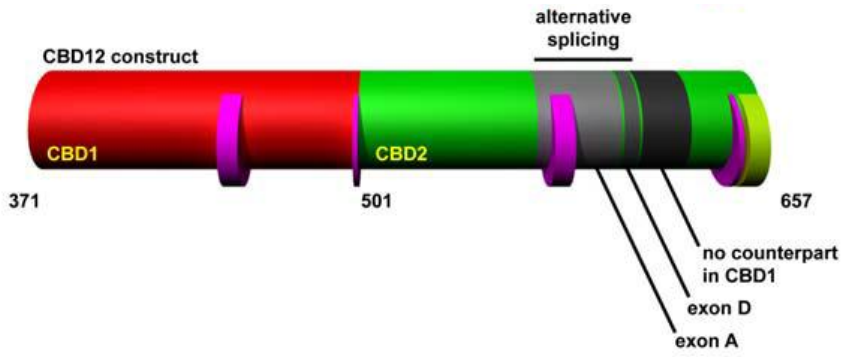

FIGURE 4. A view of NCX1.4 (CBD1 and CBD2) with the alternative splicing region highlighted. The gray and dark gray regions are included in the alternative splicing zone. In NCX1.4, exons A and D are included. Magenta regions depict the locations of acidic residues and the yellow region is the location of a region that extends beyond CBD2 and which is required for binding calcium ions. (Hilge et al. 2006)

NCX1.1 Structure

The sarcolemmal isoform NCX1.1 is of specific interest because of its necessity for cardiomyocytes. Its topology, shown in Figure 3, closely mimics those of the other NCX variants and isoforms. The full structure of NCX1.1, comprised of roughly 1000 amino acids and having a size of around 110 kilodaltons (Nicoll et al. 1990), is not specifically known. Nonetheless, previous x-ray crystallography (Mima et al. 2008; Wu et al. 2010; Nicoll et al. 2006; Wu et al. 2009) and nuclear magnetic resonance (NMR) studies of NCX1.1 and other NCX1 isoforms have revealed some structural details (Johnson et al. 2008; Salinas et al. 2011). Like other NCX proteins, NCX1.1 is characterized by two groups of transmembrane helices, one with five helices and one with four, that are connected by a long intracellular loop (Nicoll et al. 1999). As described earlier, each transmembrane section features an α site that helps open the pore and pass ions through the protein and across the membrane (Schwartz and Benzer 1997). The mechanism for this action is not yet understood, but many hypotheses focus on the intracellular loop as a regulator of ion transport.

The cytosolic loop of NCX1.1 includes two calcium-binding domains (CBD1 and CBD2) as well as an exchanger inhibitory peptide (XIP) region (Li et al. 1991), which can be seen in the topology diagram in Figure 3. The XIP region has been shown to be necessary for regulation of ion transport. This can occur by interaction with various ligands, including acidic phospholipids and sodium ions, and is regularly inhibitory, as its name suggests.

The CBDs have been the focus of many structural and physiological studies. A structure of these domains can be seen in Figure 5. The two domains resulted from a duplication event, leaving their general structures with many of the same features. Each CBD is a Calx-beta motif (Schwarz and Benzer 1997), which is mostly composed of seven antiparallel β-sheets in a sandwich formation. The two domains, CBD1 and CBD2, are connected by a short linker, or hinge, that is critically important for interactions between CBD1 and CBD2 that mediate the regulatory function of CBD1 (Wu et al. 2010; Giladi et al. 2010). Calcium ions can bind to either domain, though CBD1 can only bind four ions at once (Nicoll et al. 2006) and CBD2 is restricted to two (Hilge et al. 2006). These binding sites are located at the C-terminal region of each domain.

Each CBD also features an unstructured loop that extends from the N-terminal region. These "FG-loops," named for the splice sites that they include, are theorized to be

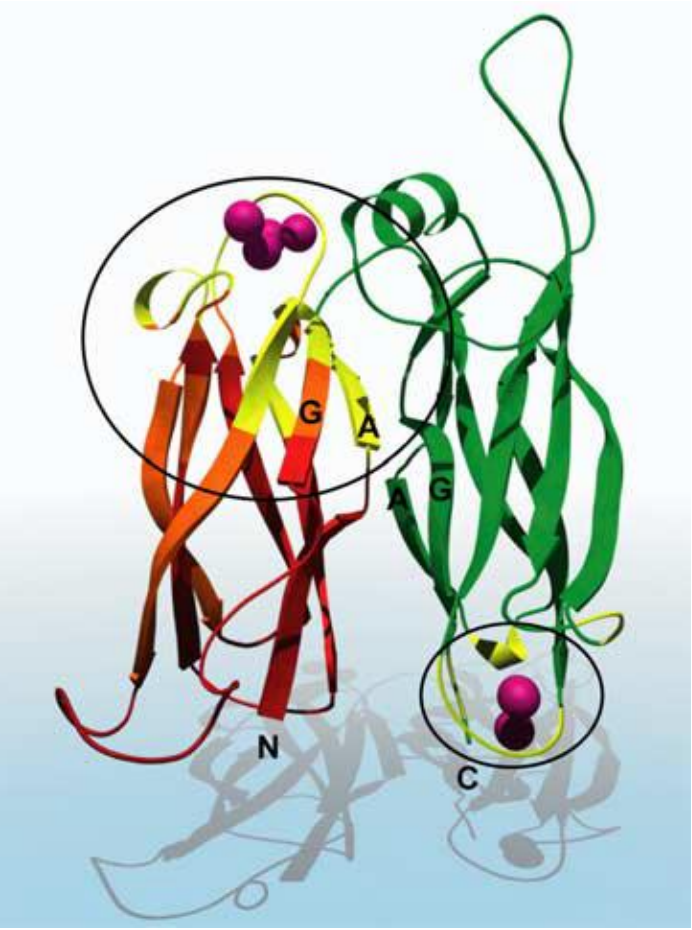

FIGURE 5. A ribbon diagram of CBD12. CBD1, left, is shown in orange/red. CBD2, right, is shown in green. The calcium-binding sites of each are shown in yellow and circled, with calcium ions displayed as fuchsia spheres. The FG-loop of CBD1 is the unstructured region at the lower left and that of CBD2 lies at the N-terminal end (top right), including the α-helix and connected unstructured region. (Hilge et al. 2007)

necessary for normal NCX1.1 function and stabilization (Breukels et al. 2010; Hilge et al. 2006). While the loop on CBD1 is relatively short, that of CBD2 extends far into the cytosol and includes a nine-amino acid α-helix. Splicing in this region results in different activity in various isoforms, including AD and BD variants (Breukels et al. 2010) as well as the ACDEF splice variant. This likely adapts NCX1 specifically to each environment

and role in whatever process each splice variant is involved in (Dyck et al. 1999). As the splicing region is present at the FG-loop of CBD2, this site is of considerable interest. Previous research has shown that the FG-loop of CBD2 can interact with the XIP region, possibly suggesting an important function for NCX1.1 activity and its mechanism (Maack et al. 2005). Conversely, it has also been determined that removing the entire FG-loop of both CBD1 and CBD2 has no effect on regulation of NCX by calcium ions (Ottolia et al. 2009). The conflicting nature of these results has made the true role of the FG-loop unclear and made future research in this area essential. Nonetheless, the flexibility of these loops makes determining a specific structure for each a difficult task.

NCX Function

No matter the variant, the general ion control mechanism is the same. A single NCX protein will bidirectionally exchange three sodium ions for one calcium ion across the cell membrane (Bers and Ginsburg 2007). In the case of NCX1.1 in cardiomyocytes, this means that the protein can assist with calcium loading for muscle contraction and calcium extrusion for muscle relaxation by transporting ions across the sarcolemma. While this is a possible function, previous research has shown that the primary activity of NCX1.1 focuses on calcium efflux, especially when the concentration of calcium ions within the cell is high (Bridge et al. 1988; Reeves and Condrescu 2003). This suggests that the reversibility of the ion exchange is secondary to a primary role of exporting calcium ions into the extracellular space following heart contraction.

The specificities of the mechanism for ion transport via NCX1.1 are not completely clear, but many aspects have been revealed by previous research. For

instance, it has been determined that the intracellular ion transport site has an affinity for calcium ions in the micromolar range and for sodium ions in the 10-20 mM range, while the extracellular site has affinities of one and 60-80 mM for calcium and sodium ions, respectively (Matsuoka and Hilgemann 1992). The binding of calcium ions to these sites is a regulatory factor for NCX1.1. Occupancy of these sites is also a limiting factor of the overall kinetic rate. However, of the six calcium-binding sites on CBD1 and CBD2, only three are essential for NCX function (Chaptal et al. 2009; Giladi et al. 2010).

There is also considerable interest in potential dimerization of NCX1.1 due to the dimerizing property of the sodium-calcium-potassium exchanger (NCKX), a related ion transporter, and many other ion transporters. It has been shown that a disulfide bond can form between the α-sites of two NCX molecules; this is a substrate-dependent process, relying on sodium or cesium ions (Ren et al. 2008). Use of FRET to study this facet has also shown that NCX can exist as oligomers. It is theorized that this oligomerization or dimerization regulates NCX activity and can effect the transportation of ions, but it is also suggested that dimerization helps to move NCX to the membrane (John et al. 2011).

Furthermore, many studies have elaborated on the integral structural pieces of NCX1 and its isoforms. As mentioned earlier, the short three- or four-residue linker connecting CBD1 and CBD2 plays an important role in NCX function. An extension of this short linker sequence with seven alanines resulted in slowed kinetics of calcium binding and removal at one of the two crucial binding sites on CBD1. However, the other two necessary calcium-binding sites (one each on CBD1 and CBD2) were independent of this change and experienced no change in kinetics (Giladi et al. 2010). Research of the involvement of cardiac NCX in the insulin signaling pathway resulted in the discovery

that the XIP region regulates NCX by binding with sites 562-679, which are part of CBD2. However, this was not true of regions on CBD1 or of other sites on CBD2 (Maack et al. 2005). Deletion of those residues also made NCX resistant to insulin-induced enhancement of the current (Villa-Abrille et al. 2008). These residues also include the FG-loop in NCX1.1, likely providing evidence that the FG-loop is important for NCX1.1 regulation. Other work focusing on the transmembrane regions of sarcolemmal NCX1

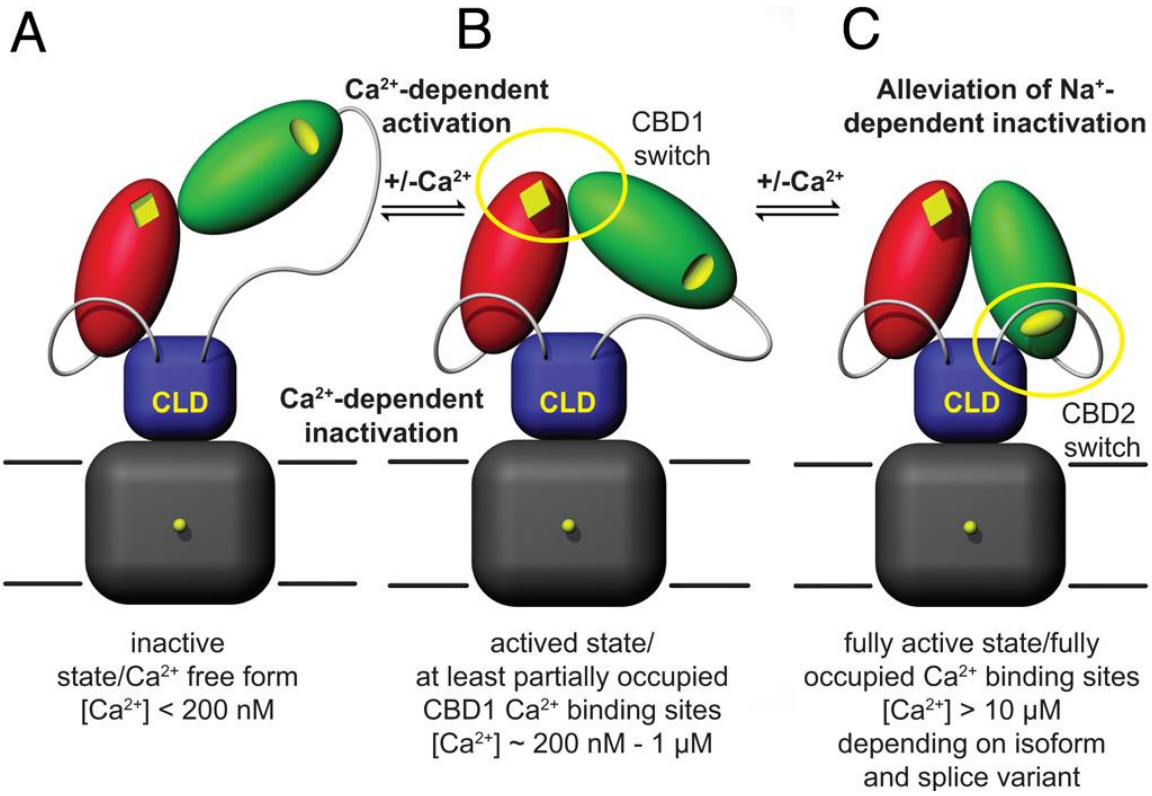

FIGURE 6. A diagram illustrating the mechanism of an electrostatic switch in NCX activity. SAXS data suggested that the domains change position relative to one another when calcium is bound. This model was then created based on the calculated movements and used to explain how NCX goes from the inactive state (A) to the compacting state with a relaxed linker region (B) and finally to the state allowing ion exchange (C). (Hilge et al. 2009).

revealed that several sites of the transmembrane helix, when mutated, could abolish or decrease NCX activity. Many of these sites are located in the α-sites, confirming the

importance of these two areas (Nicoll et al. 1996). Previous work has also suggested that CBD1 and CBD2 can flex around the linker connecting them and move relative to one another (Figure 6), and that this movement is necessary for NCX1 activity (Hilge et al. 2009).

NCX Role in Abnormal Cardiomyocte Activity

Understanding the mechanism and activity of NCX1 isoforms can provide insight into diseases and other debilitating conditions involving NCX1. In the heart, NCX1 has been shown to be involved with heart failure. Heart failure can result from a number of conditions, such as weakening of myocardial contractility or other problems, which cause abnormal blood circulation to peripheral organs (Wei et al. 2007). Most of these cases involve the cycling of calcium ions in related cells. While NCX1 is typically responsible for only 28% of calcium extrusion in healthy cardiomyocytes of rabbits (Bassani et al 1994), this increases to 49% during heart failure (Bers and Despa 2006). The amount of contribution by NCX1 differs by species, but all seem to follow this general pattern of an increase in percentage of total calcium extrusion during heart failure. This increase, likely related to an increase in NCX1 expression and/or a decrease in expression of the sarcoendoplasmic reticulum ATPase (SERCA) (Kohlhaas and Maack 2010), removes calcium ions from the cell faster than the SERCA can transport them into storage in the SR. This decreases the availability of calcium ions for the next contraction. Interestingly, this activity also means that there is a buildup of sodium ions within the cell (Louch et al. 2010), which agrees with previous reports of heart failure (Pieske et al. 2002; Despa et al. 2002). As sodium has been determined to inactivate NCX1 with high concentrations,

enough to bypass activations from calcium ions, this could be an intrinsic factor of heart failure (Reeves and Condrescu 2008). Also, a high concentration of sodium ions stimulates reverse-mode function in NCX1, bringing more calcium ions into the cell than usual. As the calcium concentration increases, diastolic calcium overload can occur, as SERCA is unable to help maintain the concentration (Pieske et al. 2002). Still, the effect of a high concentration of sodium ions on NCX1 could protect cells from extreme levels of calcium ions (Reeves and Condrescu 2008). While NCX1.1 can promote calcium overload in certain physiological conditions, other isoforms can have varied effects. For instance, NCX1.3 has shown an ability to protect against calcium overload (Hurtado et al. 2006). Because NCX1.1 is the most prevalent isoform in cardiomyocytes, its effect on the cardiac cycle is of greater interest than the effects of other isoforms.

No studies have specifically mentioned NCX1.1 as a contributor to certain diseases or disorders. Nevertheless, all three NCX proteins have been identified as potentially having roles in several medical conditions. For instance, NCX1, 2, and 3 have been shown to colocalize with amyloid-β in synaptic terminals. All three variants also experience changes in regulation in Alzheimer's disease (AD) terminals, with NCX2 showing a significant increase in expression (Sokolow 2011). NCX function has also been associated with impaired calcium homeostasis during aging of the brain (Michaelis et al. 1984; Canzoniero et al. 1992). In addition, β-amyloid peptides can aggregate and inhibit NCX activity directly (Wu et al. 1997) or cause changes in calcium homeostasis in the cell by way of other channels, creating a downstream effect on NCX (Mattson and Chan 2003). See the review by Gomez-Villafuertes, et al. for the wealth of information on the role of NCX in neurodegeneration (Gomez-Villafuertes et al. 2007).

Outside of the neural system, NCX proteins have roles in various other disorders. Blockage of NCX reverse mode can significantly reduce the incidence and severity of pilocarpine-induced seizures, which are a model for epileptic research (Martinez and N'Gouemo 2010). In addition, pentylenetetrazol-induced convulsions, another model for epilepsy, seem to be inhibited by NCX present in the hippocampus, suggesting an important role of NCX-mediated calcium influx for resisting seizures (Saito et al 2009). Another disorder, Andersen-Tawil syndrome, is also tied to NCX and may see an impact specifically from NCX1.1. Andersen-Tawil syndrome involves ventricular arrhythmias and QT prolongation (i.e., lengthening of the electrical cycle of the heart). This abnormal ventricular activity occurs primarily in areas with increased NCX expression where calcium influx is slowed (Radwański and Poelzing 2011). Another cardiac disorder, long QT syndrome, is characterized by sudden cardiac death due to syncope and a prolonged QT interval. It has been determined that inhibition of NCX decreased the pQT prolongation and was an effective way to treat this disorder, suggesting that NCX overexpression can have a severe negative effect on certain regions (Milberg et al. 2008).

All of these medical issues can be related to NCX function and activity, and it is thus imperative to understand the mechanism of NCX-mediated ion transport. This dissertation focuses on the local motions of secondary structure elements thought to be important for NCX1.1 activity. This information can reveal further details about the proteins and how their mechanisms may be related to different disorders. The use of electron paramagnetic resonance provides a sound method of exploring this mechanism and opens doors for further research into the structure and function of NCX1.1.

CHAPTER II

ELECTRON PARAMAGNETIC RESONANCE

Principles of EPR

EPR Signal

Unlike NMR, which harnesses the physical properties of nuclei to determine spectra, EPR examines the free electrons of a system. Many of the theoretical details of the two techniques are very similar, however. With an electron, the focus is primarily on the spin *S*, magnetic moment μ, and quantum number M_s, which describes the z coordinates of the electron's spin. Magnetic moments of electrons are typically randomly oriented in space, but when presented with an external magnetic field (*B*), the magnetic moment of the electron will cause its spin to line up with the field in either a parallel ($M_s = -{}^1/_2$) or antiparallel ($M_s = +{}^1/_2$) conformation. These states represent the low and high energy states of the electron, respectively. Each state has a specific energy, and this phenomenon is called the Zeeman effect (g_e). An example of the energy diagram for this process is shown in Figure 7. The magnitude of the energy difference between levels is proportional to the strength of B. The energy states can be described by the equation

$$U = -\mu_z B = g_e \beta_e B M_s$$

where *U* is the energy of the state, g_e is a Zeeman correction factor (equal to 2.002319), *e* is the electronic charge, and β_e is the Bohr magneton. The Bohr magneton is a constant representing the magnetic dipole moment of an electron, represented by this equation:

$$\beta_e = \frac{|e|\hbar}{2m_e} = 9.2740154(31) \times 10^{-24}\ \mathrm{JT}^{-1}$$

Each unpaired electron can have M_s values of $+^1/_2$ or $-^1/_2$, meaning that the following equations are true:

$$\mu_z = \mp\frac{1}{2} g_e \beta_e \qquad U = \mp\frac{1}{2} g_e \beta_e B$$

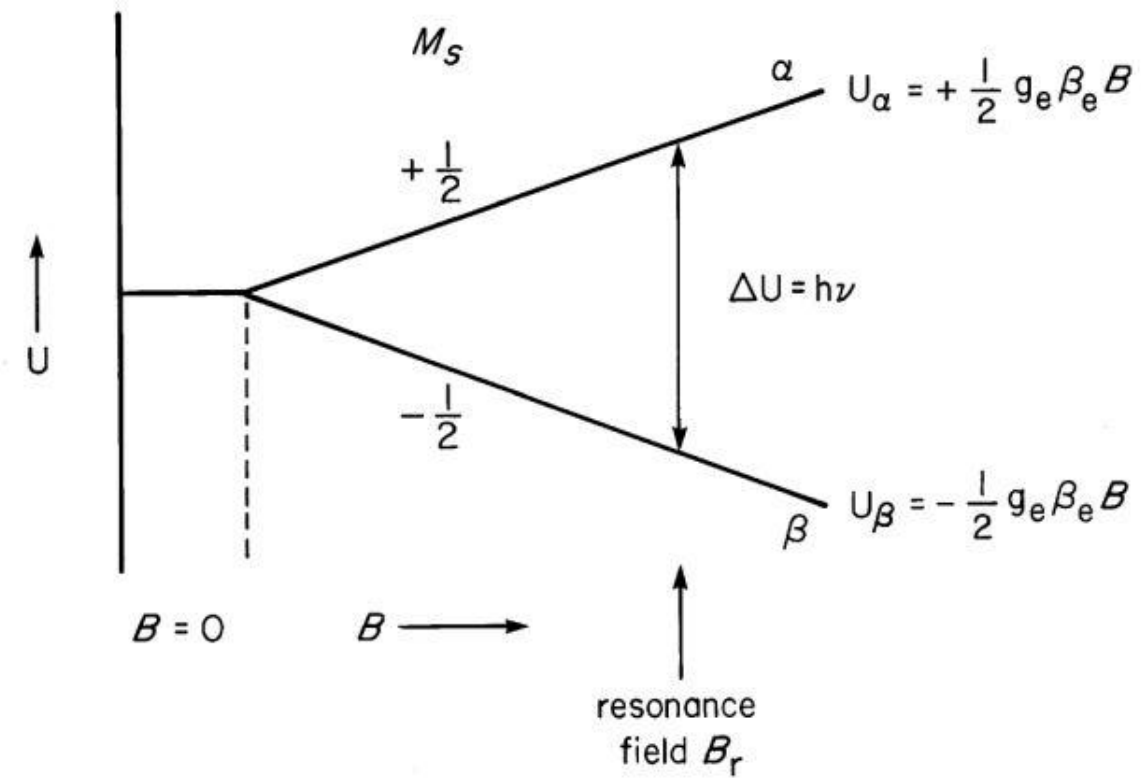

FIGURE 7. A simple example of an energy-level diagram for a free electron in an applied magnetic field *B*. The spin states M_s = +½ and M_s = -½ are represented by U_α and U_β. (Weil et al. 1994)

Free electrons can migrate between energy states by absorbing energy from the static electromagnetic field *B*, which should have a frequency *ν* that makes this equation true:

$$\Delta U = h\nu = g_e \beta_e B$$

In the case of continuous wave (CW) EPR – and for the purposes of this dissertation – the frequency of the radiation is held constant and the field varies in strength along a spectrum, called a sweep. Per the equations above, when the electromagnetic field *B* gradually increases in Gauss, ΔU will also increase until the equation above is true and the value of ΔU is identical to $h\nu$. At this point, the electrons will absorb energy and jump to the higher state, from which they can fall back to the lower state by emitting energy. This movement is recorded by the spectrometer as a change in the current flow to the detector. The detected flow is also determined by the Boltzmann distribution of spins in the system. A system's spin distribution is given by the equation:

$$\frac{N^+}{N^-} = e^{-g\beta H/kT}$$

where *N* is the population of spins in the higher (N^+) or lower (N^-) state. At room temperature, there is an excess of lower-state spins. This excess is much greater than that of NMR, ultimately providing a much better signal-to-noise ratio. The distribution of spins in the system and their movement between levels are huge contributing factors of the output spectra from EPR analysis.

The signal that results from this absorption also depends on the locations of the free electrons in the system relative to nearby nuclei and free electrons. The dipole of the free electron is sensitive to the dipoles of electrons and nuclei around it and to the directions of those dipoles. Contributions of these dipoles to the local field depend on the spin state of the central free electron. In output spectra, this effect results in multiple lines rather than one, based on the number of spin states. The lines are split further by an effect called hyperfine splitting, which is the product of interactions with local nuclei and is represented by a Hamiltonian:

$$\widehat{\mathcal{H}}_s = g\mu_B B\hat{S}_z + A\hat{I} \cdot \hat{S}$$

The symbol *A* is the hyperfine coupling parameter (joules). A free electron with one spin state and interacting with one local nuclei will result in two lines on the output spectrum. With two interacting nuclei, there are three lines, with three nuclei, four lines, and the effect continues in this pattern. Eventually, nuclei will be too distant from the free electron and the signal from those lines will be indistinguishable from background noise in the spectrum. An example of hyperfine splitting can be seen in Figure 8, which details the effects of each added interacting nucleus. This effect can be either isotropic (independent of dipole orientation) or anisotropic (splitting is dependent on the orientation of the molecule relative to the magnetic field *B*).

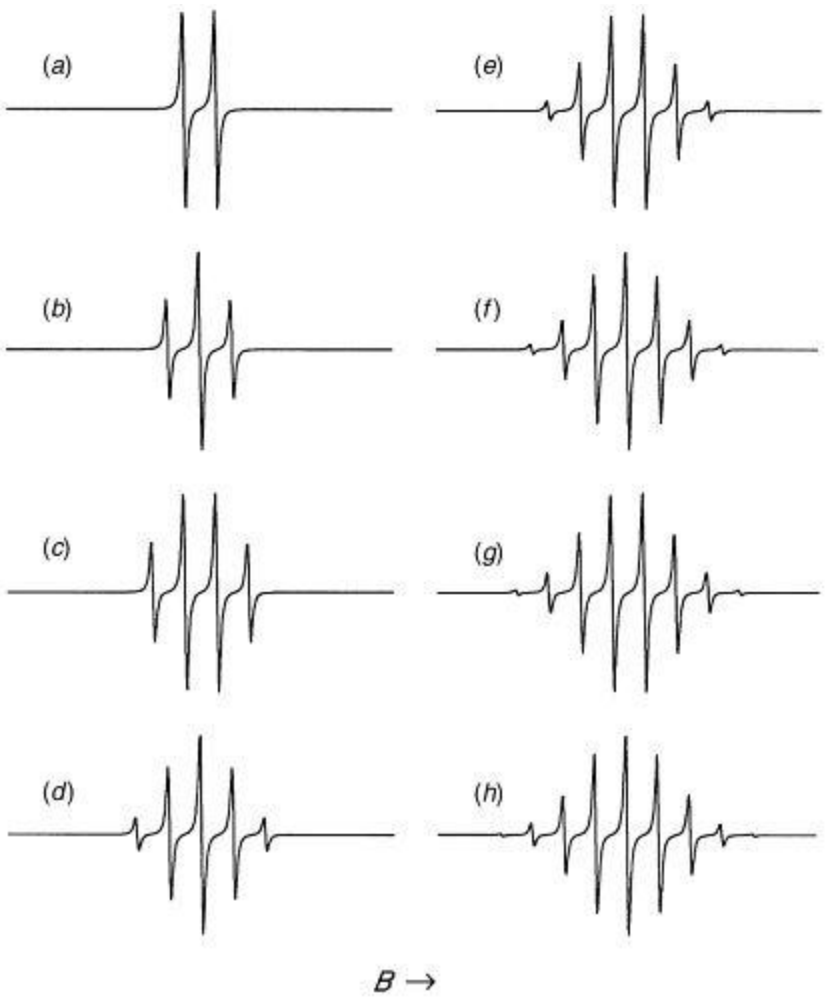

Figure 8. An example of the effect of hyperfine splitting on spectra. These computer-simulated spectra result from a single free electron that interacts with one (a), two, (b), three (c), four (d), five (e), six (f), seven (g), or eight (h) equivalent spin ½ nuclei. (Weil et al. 1994)

Other interactions that a free electron can experience involve other free electrons in the system. This situation arises when a protein includes multiple free electrons (intramolecular) or when free electrons on separate proteins are near enough in solution to interact (intermolecular). This second factor will result in line broadening in the output spectrum. The interactions between free electrons are very strong due to the large

magnetic moment of electrons. Therefore, these interactions overshadow others with their signal in the output spectra.

The intramolecular or intermolecular interactions of two free electrons through the overlap of their orbitals results in four spin states, which can be divided into a triplet state (*S = 1)* and a singlet state (*S = 0*). The separation in energy between these states is ruled by the electron-exchange interaction, which is mathematically expressed with a spin Hamiltonian:

$$\widehat{\mathcal{H}}_{exch} = \sum_{ij} J_{ij}\hat{S}_{1i}\hat{S}_{2j} = \frac{1}{2}\left(\hat{S}_1{}^T \cdot J \cdot \hat{S}_2 + \hat{S}_2{}^T \cdot J^T \cdot \hat{S}_1\right) \qquad i,j = 1,2,3$$

In this equation, $\hat{S}_1$ and $\hat{S}_2$ are electron spin operators for the two interacting electrons, while *i* and *j* label spacial coordinates. In this version, *i* and *j* are limited to 1, 2, or 3 in order to fit *J*, which is a matrix of three rows by three columns in this case. An important note is that this equation focuses on the electric interactions between the electrons themselves and excludes any magnetic interactions. When dipole-dipole interactions are also considered, the spin Hamiltonian can be expressed as such, where *D* is the parameter matrix:

$$\widehat{\mathcal{H}} = g\beta_e B^T \cdot \hat{S} + \hat{S}^T \cdot D \cdot \hat{S} + \frac{1}{2}J_o\left[\hat{S}^2 - \frac{3}{2}1_3\right]$$

Ultimately, when electrons are excited, their relaxation times can be characterized by τ_1 and τ_2. Spin-lattice relaxation time, τ_1, is the time it takes for the spin-orientation states to return to equilibrium while interacting with the local lattice. The second variety, spin-spin relaxation (τ_2), describes spin diffusion and other processes that alter ΔU rather than the time it takes for the electrons to relax. In the case of EPR, free

electrons on the nitroxides of spin labels have a τ_2 of roughly 100 nanoseconds and a τ_1 in the microsecond range.

Spin Dynamics

Output spectra from EPR runs exhibit a number of features that relate to the sample's structure and its interaction with the solution, or lattice, around it. For instance, if the free electron on the molecule is able to freely rotate, the resulting spectra will have very sharp, well-defined lineshapes. Other factors, like constrained rotation, reactions with other molecules, and molecular tumbling, can result in specific changes in the spectra. Line broadening of the spectra can occur depending on the factors at play in the sample, and this effect can be of two types. The first, homogenous line broadening, occurs when spins in the sample are exposed to the same net magnetic field and have the same set of spin-hamiltonian parameters. Essentially, each dipole experiences the same environmental effects and thus produces the same line broadening effect. Conversely, inhomogenous line broadening occurs when all of the dipoles in a sample are exposed to different *B* values. The line broadening in this case does not result from equivalent spins, as the magnetic field is not at the correct frequency for every spin to react. Other causes include unresolved hyperfine structure, anisotropic interactions in a solid state, and dipolar interactions between fixed paramagnetic centers.

Motions in a sample during EPR scans can be on a range of fast to slow. Fast motions are associated with correlation times of less than one nanosecond for typical 1- to 100-GHz frequency EPR spectrometers. These fast motions, which include those of side chains, narrow features of spectra by averaging anisotropic magnetic interactions.

Slightly slower, or intermediate, movements (1-10 nanoseconds) only partially average anisotropic magnetic interactions. This effect, and the constant magnetic field of the spectrometer, leads to homogenously broadened spectra. Intermediate motions include tumbling of globular proteins and the motions of exposed, unstructured loops. Slow motions on the ten-nanoseconds-to-one-microsecond scale resolve features of the output spectra that exhibit anisotropic magnetic interactions and their size. These typically involve tumbling of larger globular proteins. Even slower motions with greater than one microsecond correlation times show rigid limits in spectra and are characteristic of proteins in a membrane or some conformational changes. In this way, EPR can resolve many biological, chemically, and physically relevant motions in a sample.

Continuous Wave and Pulsed EPR

Continuous wave EPR (CW-EPR) irradiates samples at a constant frequency to keep the sample at equilibrium. The electromagnetic field is varied along a spectrum to produce spectra. A sample sits in a resonator cavity, where the external field is applied and built up. When the electrons absorb and release energy to rise to and fall from high energy levels, this reflected power is measured by the detector as a function of the applied field. This, in turn, produces the CW-EPR spectrum.

Conversely, pulsed EPR is more reflective of NMR techniques. Pulsed EPR uses an electron spin echo technique with pulse sequences to orient electrons' spins and measure the echoes of emitted energy as they relax. EPR pulse sequences commonly include two pulses, one at $\frac{\pi}{2}$ and one at π. This pulse sequence will affect the sample in the progression shown in Figure 9. For example, before initiating the sequence ($t < 0$), the equilibrium magnetization M_0 of the sample spins exists along the z-axis. When the $\frac{\pi}{2}$ pulse is applied at $t = 0$, the spins align 90° away. In the time following, the spins

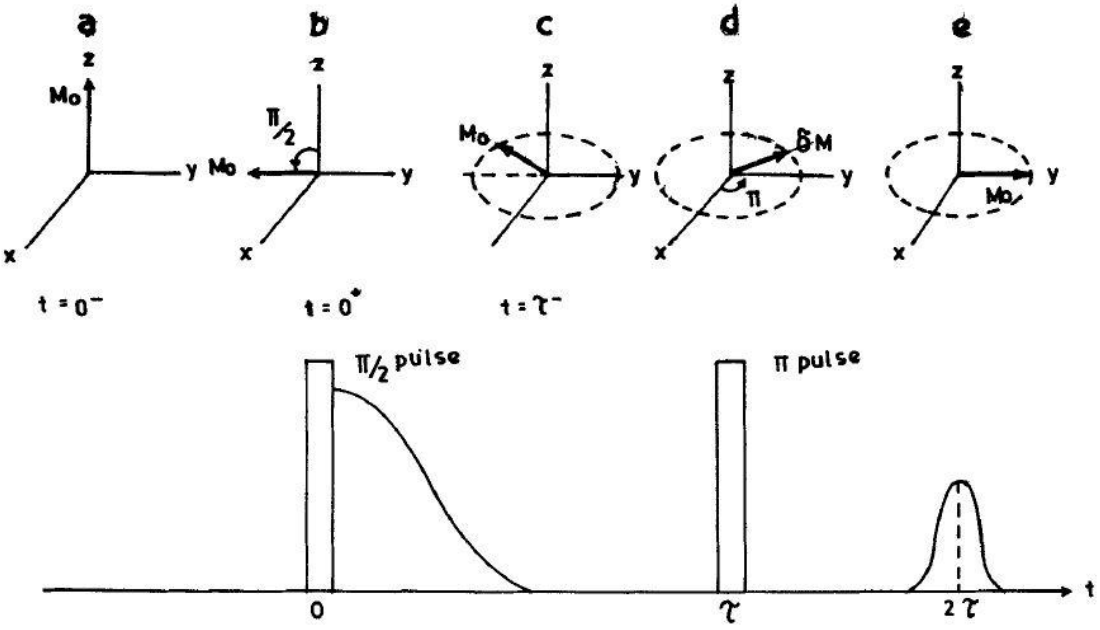

FIGURE 9. The effects of a two-pulse technique – featured at bottom with pulses, decay, and echo – on the magnetization vector M_0. (a) shows the initial vector position along the z-axis. Following a $^{\pi}/_{2}$ pulse, M_0 moves 90° to sit along the y-axis, as shown in (b). During the time between pulses, the vector defocusses in the x-y plane, seen in (c). After the π pulse, (d) features the refocussing of M_0 before the echo formation, shown in (e). This final echo is measured by the detector. (Sunandana 1998)

randomly orient in the x,y-plane during defocussing. A full π pulse then flips the spin orientations and refocussing occurs as the magnetization is returned to normal. The normal magnetization allows for the determination of relaxation times. These experiments are performed at low temperatures (80 K) in order to slow motion and relaxation to measurable times. Like NMR, a variety of pulse sequences can be used for various situations and samples

The microwave pulses used for pulsed EPR come with a drawback. Because these pulses typically do not excite the whole spectrum concurrently, pulsed EPR is less sensitive than CW-EPR. Another problem pulsed EPR can face is the quick relaxation times, which are faster than those of NMR and result in lost information. Even with these drawbacks, however, pulsed EPR can parse out various interactions or types of spin relaxation mechanisms better than CW-EPR.

Introduction and Use of Spin Labels in EPR

Site-Directed Spin Labeling

In order to control the location of free electrons in a sample, most studies of proteins and biological systems use spin labels that can be manually attached to specific sites. These labels are chemically designed to include a free electron and to be easily attached to proteins or compounds. In many cases, the methanethiosulfonate spin label (MTSSL) is used for protein complexes, the structure of which can be seen in Figure 10. MTSSL results in a typical output of three lines, as shown earlier in Figure 8b, because the free electron sits on a nitroxide. The four methyl groups on the pyrroline-type ring

help to stabilize the nitroxide group and protect it from reducing to hydroxylamine when in contact with a reducing agent. The sulfur of MTSSL allows for disulfide bonds with

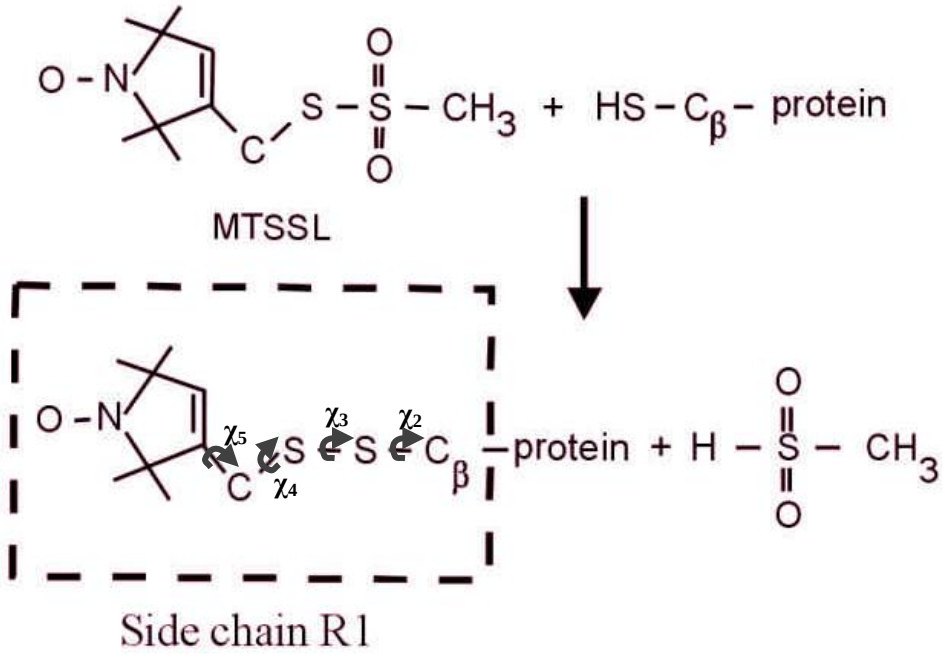

FIGURE 10. The chemical structure of MTSSL and the reaction to form a disulfide bond with the sulfur of a cysteine residue. The bonds around which movement takes place, χ_2, χ_3, χ_4, and χ_5, are shown on the R1 diagram. (Steinhoff 2002)

cysteine residues when exposed to protein samples.

A primary use of MTSSL with proteins is the ability to introduce or define locations of cysteines in order to study specific areas or dimensions of the protein. Using side-directed mutagenesis techniques, all endogenous cysteines of a protein can be replaced with small residues such as alanine. When all cysteines are removed, new cysteine residues can be added using mutagenesis to ensure specific labeling and analysis of areas of interest. This is the basis of site-directed spin labeling (SDSL). When using this technique, it is important to ensure that all removed and introduced cysteine residues

do not perturb the structure or function of the protein, so that normal measurements can be taken. In many cases, removing free cysteines, those not normally bound in disulfide bonds, introduces little to no negative effects. This further strengthens the case of SDSL with EPR as a method of focused analysis of proteins of interest.

Mobility of Attached Spin Labels

Like any side chain of an extended amino acid, MTSSL attached to a cysteine residue can move in many directions. Figure 10 shows the bonds around which rotation and general motion can occur. Generally, most of the spin label motion is defined by bonds χ_4 and χ_5 because these bonds are positioned nearest to the nitroxide. This also results from rigidity around the bond between the sulfur and α-carbon of the cysteine residue. On a very basic level, the rotation and motion of the spin label itself can be seen in the correlation time of output spectra, with fast motion corresponding to fast correlation times and slow motion to slow times. These motions occur on the nanosecond time scale and define the overall shape of the output spectra. The relation of side chain mobility to spectrum shape is shown in Figure 11. As is evident in the figure, free MTSSL produces three clean, tall, well-defined lines, while the lines become more restricted and broad as spin label mobility is limited. In terms of protein structures, a spin label that sits on an unstructured loop in solution will often show high mobility, while a label that is in a highly-ordered and packed region will show restricted motion in its spectrum. This is the simplest way to qualitatively understand a protein's characteristics in a certain region.

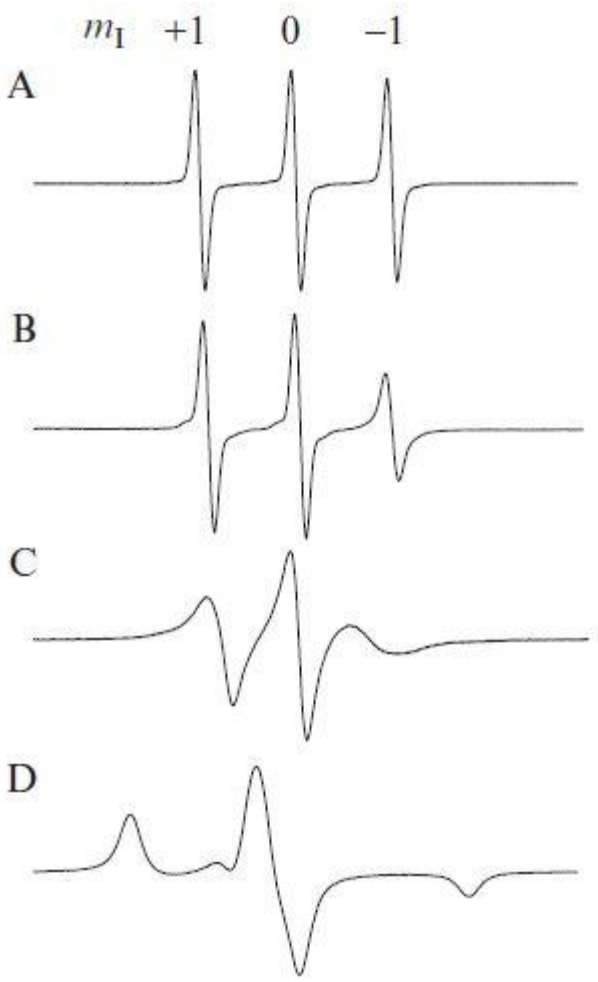

FIGURE 11. The changes in lineshape as mobility of the spin label decreases. In (A), the MTSSL is simply free in solution. (B) shows the lineshape of MTSSL bound to a 15-residue peptide. (C) is the resulting lineshape from MTSSL bound to and folded into an α-helix. Finally, (D) is a frozen sample of MTSSL. (Klug and Feix 2008)

On the molecular and macromolecular scale, MTSSL attached to cysteine of a protein can produce a spectrum that reflects protein tumbling, interactions with other molecules or structures, and the general arrangement of local structure. Most of the tumbling that occurs must be on smaller proteins to be visible in the spectrum, as large proteins and complexes tumble far too slow to be easily distinguished. However, any contributions to the spectrum from small tumbling proteins can be removed by

introducing a viscous solvent to the sample solution, effectively limiting the tumbling speed. As described above, interactions with other molecules or secondary structural elements of a protein can reduce motion of a spin label. This effect can be seen in the resulting complicated spectra that can near the rigid limit. Qualitatively, this provides many details about the local environment, but simulating EPR spectra can provide more specific ideas of backbone and sidechain structure around the spin label. Because of the rigidity of the sulfur-α-carbon bond, motion of the spin label can often correlate to movement of the protein backbone. This provides even more information about any local motions that define the protein's structure.

Distances Between Spin Labels

The standard use of EPR in this dissertation, as in many studies, is examining distances between spin labels added to one or more proteins of interest. This is used for many purposes, including the measurement of conformational changes, standard structural dimensions, and the binding of macromolecular complex subunits. Both CW-EPR and pulsed EPR can be used for this, with CW-EPR able to detect distances in the range of roughly 10-25 Å and pulsed EPR for about 20-80 Å. The interactions between free electrons provide the distance information for this experiment. The reliance on knowledge of the spin labels' location means that MTSSL's inherent ability to move and flex introduces another variable. Without exact knowledge of each spin label's orientation, resolution of the distance for building structural representations can be less than optimal. Still, with many programs developed to interpret the spectra and produce distance information, rough-to-highly specific distance ranges can be determined.

In CW-EPR, interactions between electrons cause line broadening in output spectra. For pulsed EPR experiments, the dipole-dipole coupling has to be isolated from other contributors to the spin Hamiltonian. Other pulse sequences may also have to be used in order to find as much detail in the spectrum as possible and to determine shorter or longer distances, as necessary. Because sensitivity of the experiment decreases as the distance between labels increases, changing the timing and arrangement of the pulse sequence can improve resolution and sensitivity.

CHAPTER III

SECONDARY STRUCTURE MOTIONS OF NCX1.1 UPON BINDING OF CALCIUM IONS

Introduction

Cardiomyocyte systole and diastole are characterized by changes in ion concentrations that cause contraction and relaxation of cardiac muscle. Action potentials in cardiac tissue cause the systolic release of calcium ions into the cytosol of cardiomyocytes, leading to contraction of the muscle. After contraction causes the expulsion of blood into the aortas leading from the heart, calcium must be removed to allow blood to reenter the ventricles and prepare for another contraction. Ion transporters are integral for this process, allowing calcium into the cytosol before contraction and expelling it afterwards. The L-type calcium channel and ryanodine receptor (RyR) are responsible for calcium influx from the extracellular environment and SR. Conversely, most of the calcium expulsion occurs via NCX1 and SERCA, extruding ions across the sarcolemma and into the SR, respectively. NCX1, in particular, has become a protein of interest due to its variants and presence throughout the mammalian body.

NCX1 is an antiporter that transports three sodium ions for every calcium ion, but it can move these ions bidirectionally across the membrane. Roughly 1000 amino acids and 110 kilodaltons in size, the isoform NCX1.1 is the primary transporter in cardiomyocytes. It features two transmembrane domains, one with five α-helices and one with four, separated by a long intracellular loop. Each transmembrane domain features an

α-site (α-1 and α-2) that are conserved among NCX proteins and other proteins in the SLC8 superfamily. These sites form the ion binding pocket for ion exchange. The intracellular loop features three domains of interest, including the exchanger inhibitory peptide (XIP) domain and two β-motifs, which likely resulted from a gene duplication event. These β-motifs, called calcium-binding domains (CBD1 and CBD2), are each composed of a seven-strand β-sandwich and are linked by a short hinge region. CBD1 can bind four calcium ions at its C-terminal region and CBD2 can bind two, though only three binding sites (two on CBD1 and one on CBD1) exhibit strong affinities. The sandwich structures undergo little to no drastic conformational change upon binding of calcium ions, but little is known about the structure of the long FG-loop of CBD2. This loop is an alternative splicing site, and NCX1.1 features a longer loop than those of other NCX1 isoforms. Included in this loop is a nine-residue alpha helix, the function of which is also unclear. Previous research has suggested that this region is necessary for NCX1 function.

Previous structural research of NCX1.1 and other NCX1 isoforms has mostly focused on individual constructs of CBD1 or CBD2, or on the joint CBD12 region, including the linker between the two domains. Recent DEER research has shown that, contrary to prior belief, the two domains do not move relative to one another when calcium ions bind. However, less is known about the specific movements and functions of the FG-loop and corresponding α-helix of CBD2 relative to both CBD2 and CBD1.

Experimental Methods

Protein Preparation and Purification

The CBD12 construct was previously designed from full length rat NCX1.1 cDNA, which was provided by Dr. J. Lytton at the University of Calgary. An ACDEF splice variant was produced and the QuikChange Site-Directed Mutagenesis Kit (Stratagene, La Jolla, CA) was used to produce cDNA of residues 360-685 with a histidine tag for use with Ni-NTA resin. This region was ligated into the pET19b+ expression vector (Stratagene, La Jolla, CA) by way of Nde I and Xho I sites. The construct included four endogenous cysteines, which were all replaced with alanine residues for the ΔC-CBD12 construct. In order to add spin labels for EPR analysis, cysteine residues were added at desired sites. All created mutants were confirmed by DNA sequencing and transformed into DE3 pLys-s *Escherichia coli* cells (Stratagene, La Jolla, CA).

Plated DE3 cells were inoculated into 50 mL of LB medium for overnight culture at 37° C and used to inoculate one liter of LB medium following growth. The one-liter culture was grown at 37° C for 2.5-3 hours or until the optical density reached roughly 0.8. Cultures were cooled by incubation in ice water for twenty minutes and induced with 1 μL 100 mM IPTG, followed by incubation for four hours at 25° C. Cells were pelleted by centrifugation at 4,000 rpm for 15 minutes and resuspended in 100 mL lysis buffer (20mM Tris-base, 300 mM NaCl, 16 mM imidazole, pH 8.0), to which 0.2 mM DTT, 40 units/mL lysozyme, 0.1 mM PMSF, and EDTA-free protease inhibitors (Roche, Indianapolis, IN)) were added. All resuspended cells were then frozen at -80° C.

Cell suspensions were slowly thawed in cool water and sonicated for two minutes while on ice. Lysates were then incubated with 1% (weight/volume) Triton X-100, 0.5 units/mL DNase, and 0.5 units/mL RNase for a half hour of nutation at 4° C followed by centrifugation for 30 minutes at 12,000 rpm (JA-20 Beckman rotor, Beckman Coulter, Inc., Indianapolis, IN). Pellets were discarded and supernatant was incubated with 1.5 mL of Ni-NTA resin (Qiagen, Valencia, CA), which had been equilibrated with previously-mentioned lysis buffer plus 1% (w/v) Triton X-100, for one hour at 4° C. Supernatant and resin was then added to columns and washed with 150 mL wash buffer (20 mM Tris-base, 150 mM NaCl, 16 mM imidazole, pH 7.5). Mutant protein samples were incubated with 10-fold excess methyl methanethiosulfonate spin label (MTSSL: Toronto research chemicals, North York, ON, Canada) overnight at 4° C.

Labeled protein was washed with 150mL wash buffer (20 mM Tris-base, 16 imidazole, pH 7.5) followed by 30 mL of a second buffer (20 mM Tris-base, 60 mM imidazole, pH 7.5). After 10 minutes of incubation with 14 mL of elution buffer (20 mM Tris-base, 250 mM imidazole, 2 mM CaCl, pH 7.5), proteins were eluted and concentrated to one mL using 30 kDa Amicon Ultra centrifugal filters (Millipore, Bedford, MA). Samples were further purified using a DEAE anion exchange column (TSK DEAE 650M; Ace Scientific, Cherry Hill, NJ) using a linear 0-0.8 M NaCl gradient. After collection of labeled proteins at the main peak of the elution profile, samples were concentrated to about 500 µL using 30 kDa Amicon Ultra filters. Protein concentrations were calculated using a UV spectrometer at 280 nm and sample concentrations were adjusted for optimal EPR sample concentration.

CW-EPR Analysis

CW-EPR spectra were collected at X-band (9.8 GHz) using a Bruker EMX spectrometer with a TM_{110} cavity (BrukerBiospin, Billerica, MA) at room temperature. Spectra were collected at 100 kHz with 5 mW microwave power and 1 Gauss field modulation (peak-to-peak). Samples were analyzed in 50 μL glass capillaries (Kimble Glass, Inc., Vineland, NJ) and sealed with Critoseal sealant (Fisher, Pittsburgh, PA). All samples were prepared in buffer with 20 mM Tris-base and 150 mM NaCl, pH 7.5. Two samples for each protein construct were created for EPR analysis: one was incubated for 10 minutes with 10 mM $CaCl_2$ (calcium-bound state) and one with 10 mM EDTA. Samples with two spin labels on the α-helix were analyzed at 2° C in 50% glycerol. Output spectra were analyzed using the previously-described convolution method (Hustedt et al. 2006; Rabenstein and Shin 1995) that assumes Gaussian distance distributions.

Pulsed EPR Analysis

Pulsed EPR (DEER) spectra were collected at X-band (9.5 GHz) using a Bruker EleXsys 580 spectrometer with a Bruker split ring resonator (ER 4118X-MD5). Analysis was completed with a standard four-pulse sequence with a 32 ns π pulse and a 16 ns $\frac{\pi}{2}$ pulse at 80 K. Samples were in 20 mM Tris-base and 150 mM NaCl, pH 7.5, with 30% (w/v) glycerol. Protein concentrations were in the 200-300 μM concentration range. Each protein was separated into two samples: one was incubated for 10 minutes with 10 mM $CaCl_2$ and one with 10 mM EDTA. Roughly 60 μL of sample was loaded into 2.4 mm i.d. quartz capillaries (Wilmad LabGlass, Buena, NJ). DEER spectra were analyzed with

in-house software. This software fits the background signal as a function of the effective spin concentration and of the radius of the molecule or complex. Meanwhile, it determines specific interactions of interest by using a distance distribution defined by Gaussians (manuscript in press). All DEER data shown have had background noise removed following analysis. Results mirrored those from the typical Tikhonov method (Chiang et al. 2005).

Results

α-Helix Stability

In order to probe the importance of the short α-helix in the FG-loop (see structural model in Figure 5) for NCX1.1 and its function, spin labels were attached at various sites along its nine-residue sequence on a construct of CBD1 and CBD2, linked by their normal hinge region. As α-helices do not necessarily keep their structure and can bend or flex, initial studies explored the stability of this helical region upon binding of calcium. Constructs with both single and double cysteine additions were analyzed to record any changes in structure.

Constructs with single spin label additions at a variety of sites (659, 662, 665, 667) showed no significant change to local structures. EPR spectra from analysis at 2° C with and without calcium ions bound were roughly the same, as is apparent in Figure 12. This provides an initial assessment of stability in the helix.

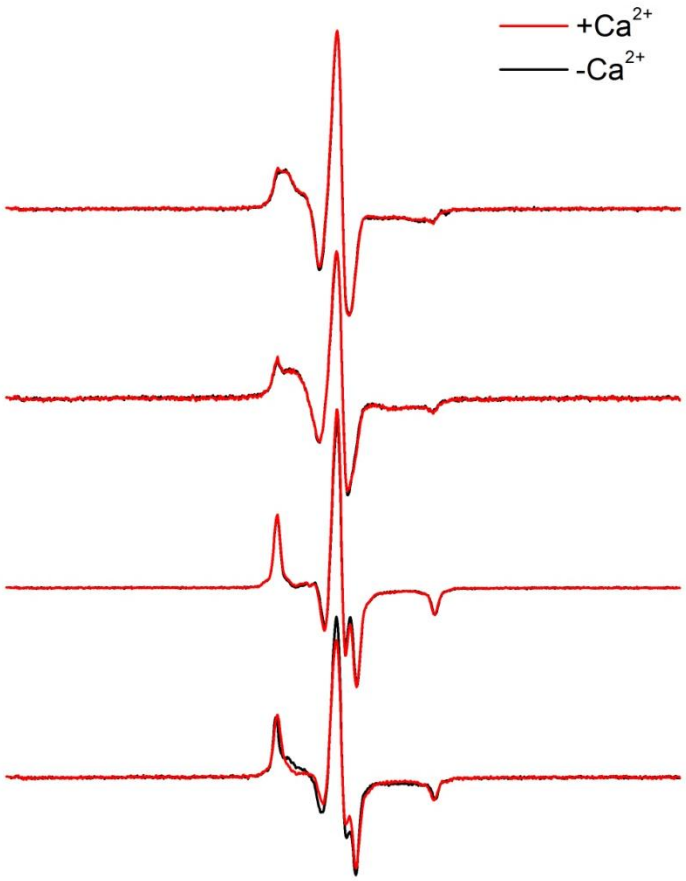

FIGURE 12. Low-temperature (2° C) CW-EPR spectra of labeled sites 659, 662, 665, and 667, all in the α-helix. The red spectra were taken from samples that had been incubated with 10 mM $CaCl_2$ and the black spectra resulted from samples that were incubated with 10 mM EDTA. There is little to no change in any of the samples, suggesting the α-helix is stable and does not rearrange upon binding of calcium.

Double-cysteine mutant constructs with added cysteines composing three different ranges (659-662, 659-665, and 662-667) were used to further measure helical stability (Figure 13). EPR analysis at 2° C resulted in spectra that showed little change between calcium-bound and -unbound states. Further analysis of the spectra yielded distance distributions (Figure 14) that exhibited no change in measured distances. These results demonstrate that the α-helix is stable in both calcium-bound and -free states.

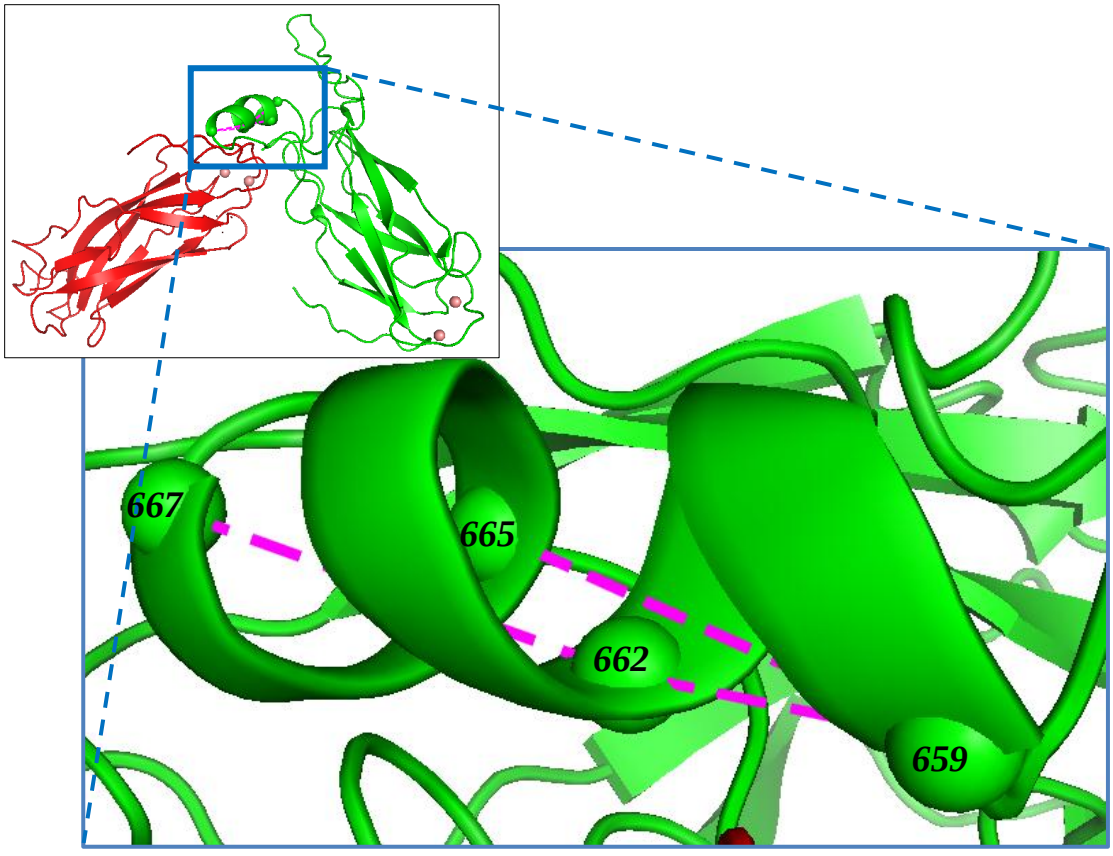

FIGURE 13. A structural diagram of the α-helix location and location of measured distances on the helix. The inset shows the full structure of CBD12 with the helix located within the indicated region (blue box). Salmon-colored spheres in the inset denote locations of calcium ions when bound. The larger image focuses on the α-helix and the distances measured with low temperature CW-EPR. Three distances, 659-662, 659-665, and 662-667, were measured and these measurements are represented by dashed magenta lines. Sites of introduced MTSSL are shown as spheres.

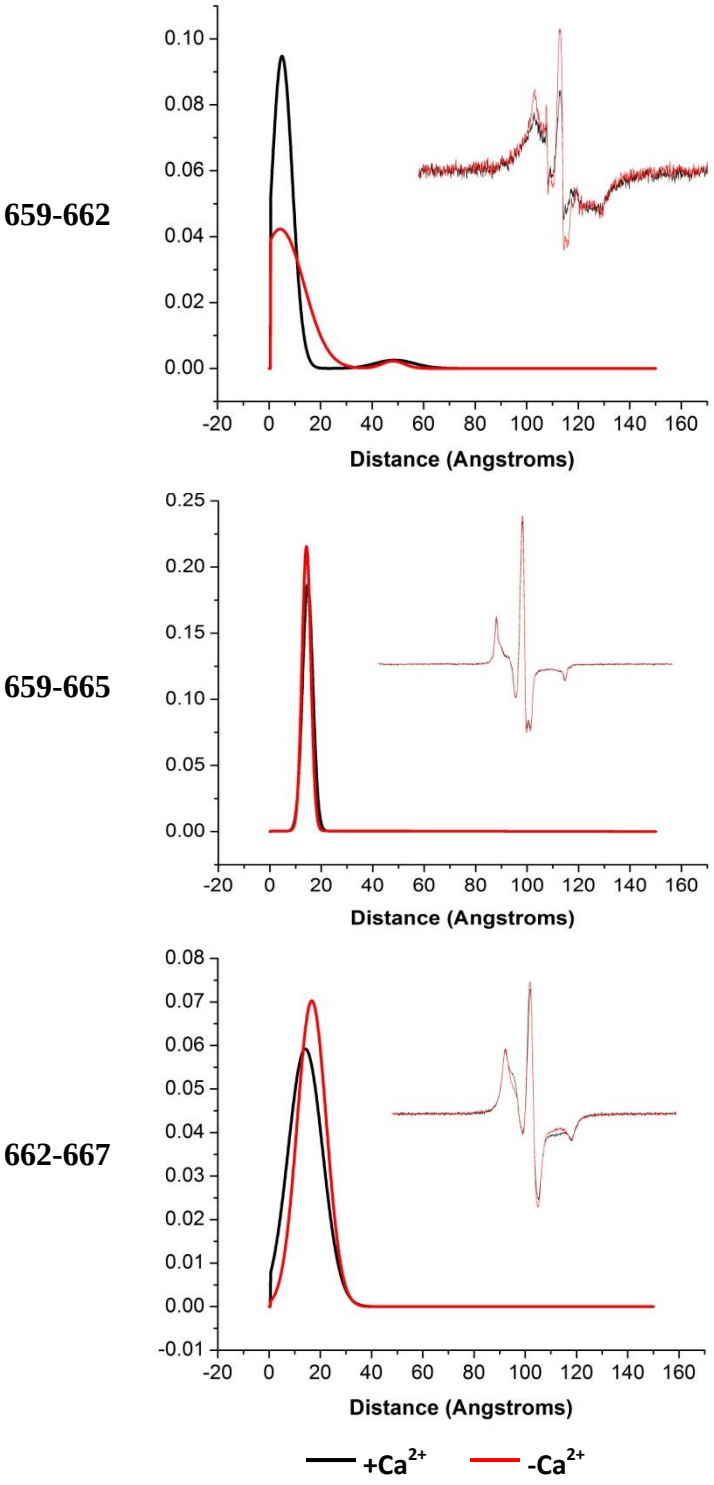

FIGURE 14. Distributions of determined distances for 659-662, 659-665, and 662-667. The insets feature low temperature CW-EPR spectra for each sample. For both distance distributions and inset spectra, black lines denote proteins that have been incubated with $CaCl_2$ and red lines are those incubated with EDTA.

Movements of α-Helix Upon Calcium Binding

Because we can assume the α-helix keeps its structure and MTSSL added at sites along it do not show great flexibility, further distance analysis can provide data about the movement of the helix during binding of calcium ions relative to CBD1 and CBD2. It was hypothesized that the α-helix may shift its position toward the CBD1 calcium-binding site upon binding of calcium ions. As previous studies of NCX1.1 had not explored the movements of the short helix, we made double-cysteine mutants between the helix and CBDs to track any movements with calcium binding.

Double mutants were made between sites 659, 664, and 667 on the α-helix and sites 384 and 457 on CBD1 and 506, 526, and 557 on CBD2. Six doubly-labeled samples were analyzed: 384-664, 457-664, 506-664, 526-662, 557-659, and 557-667. These connections to both CBDs allow us to understand and follow any movements of the helix relative to both domains (Figure 15). Pulsed EPR analysis was used to analyze each of these double mutants and computer analysis simulated likely distances between each pair. Output spectra from double mutants are shown with distance distributions in Figure 16. The data suggest that there is potentially more movement of the α-helix than previously known, but the range of distance changes and the direction of movement seem to be inconsistent between data. Three double mutants including site 664 show considerably more distance changes than the other two double mutants, suggesting either local backbone or spin label motions or a change in total orientation of the CBDs and helix relative to one another.

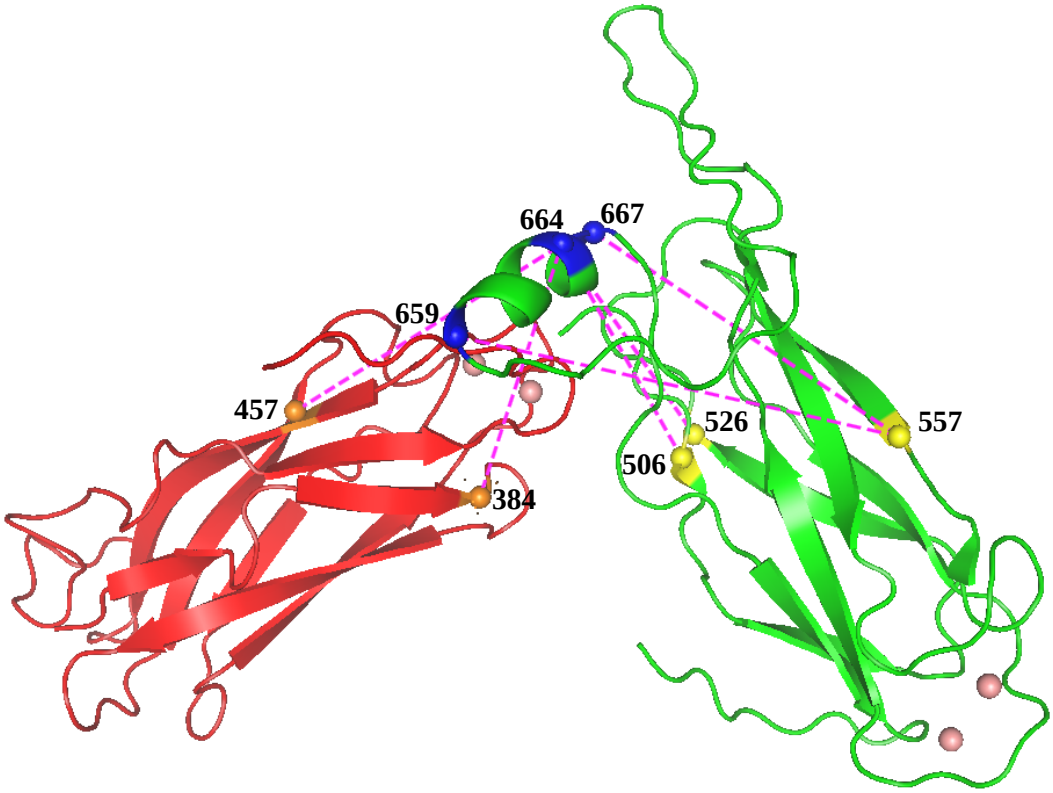

FIGURE 15. The measured distances from the α-helix of CBD2 to sites on both CBD1 (red) and 2 (green). Magenta lines mark the measured distances. Orange and yellow spheres mark included sites from CBD1 and CBD2, respectively. Blue spheres mark included sites on the helix. Salmon spheres denote locations of calcium binding.

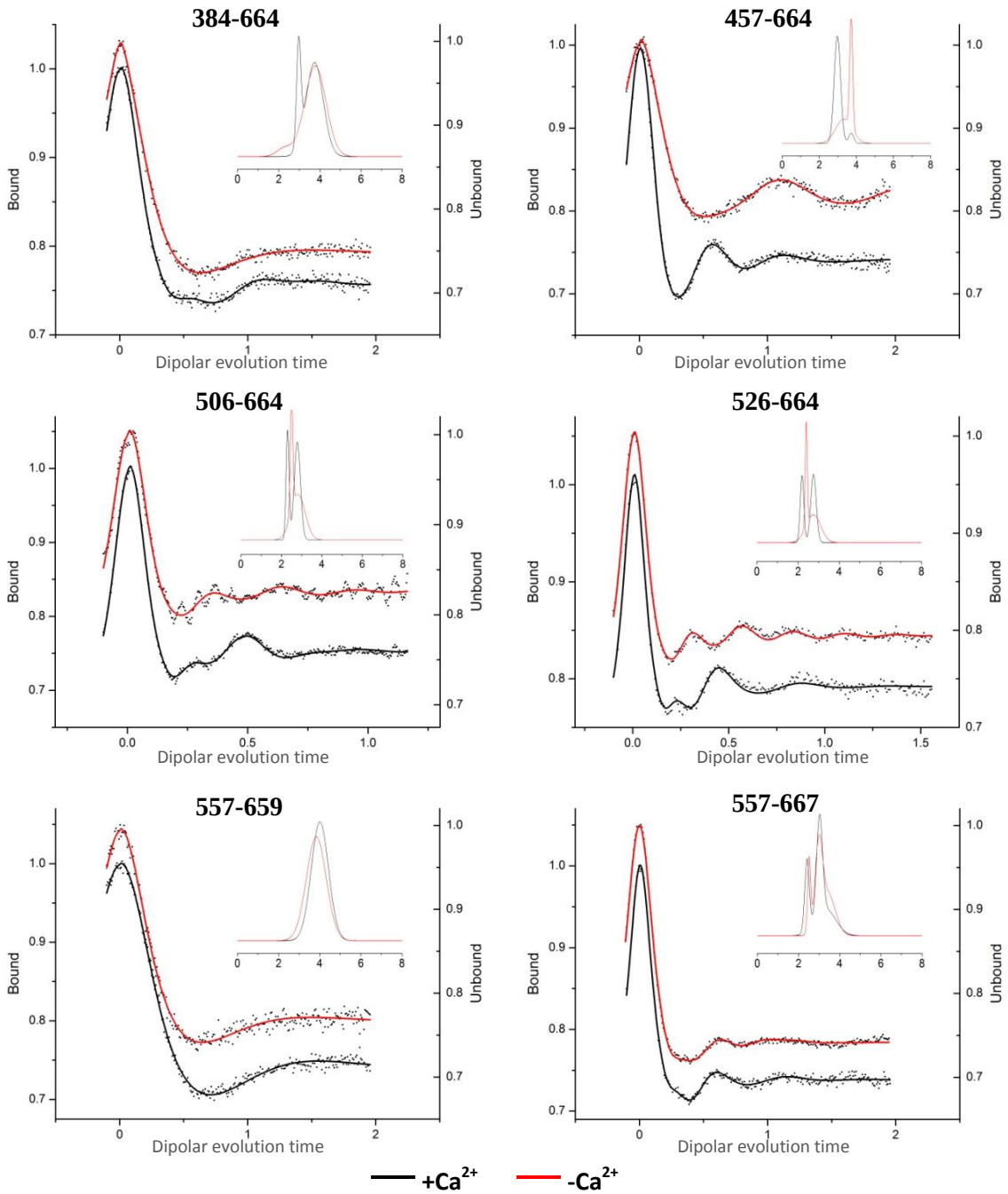

FIGURE 16. Pulsed EPR spectra of analyzed double mutants including sites on the α-helix and on either CBD1 or CBD2. The inset of each shows the calculated distance distribution in nanometers for both calcium-bound (black) and -unbound (red) samples. Y-axes on the left (calcium-bound) and right (calcium-unbound) denote the time domain signal.

Flexibility and Motion of FG-Loop

The FG-loop of CBD2 in NCX1.1 has been predicted to interact with the XIP region upon calcium binding, suggesting some small- and/or large-scale conformational change to accomplish this. In terms of secondary structure, the FG-loop is long and extended, meaning that previous NMR experiments have not seen a static structure but instead a very flexible one. Also, the entire loop had to be removed for x-ray crystallography analysis of CBD2 due to its destabilizing effects during crystallization. These factors have introduced such variability or problems for structural techniques that not much is known about the motions of the FG-loop during NCX1.1 function.

Both CW- and pulsed EPR were used to explore movements of the greater FG-loop outside of the α-helix discussed in the previous results section. Several sites along the loop were selected for distance measurements to both CBD1 and CBD2: 615, 620, 625, 629, 635, 640, 645, and 650. Single-mutant CW-EPR spectra were taken for a mutant of each site (except 650), and most followed a consistent pattern. When calcium ions are not bound, there is fairly free MTSSL motion. However, when calcium ions bind to CBD1 and CBD2, the lineshapes are more restricted. This suggests that binding of calcium causes a change in local environment in some way, resulting in a limitation of spin label motion (Figure 17).

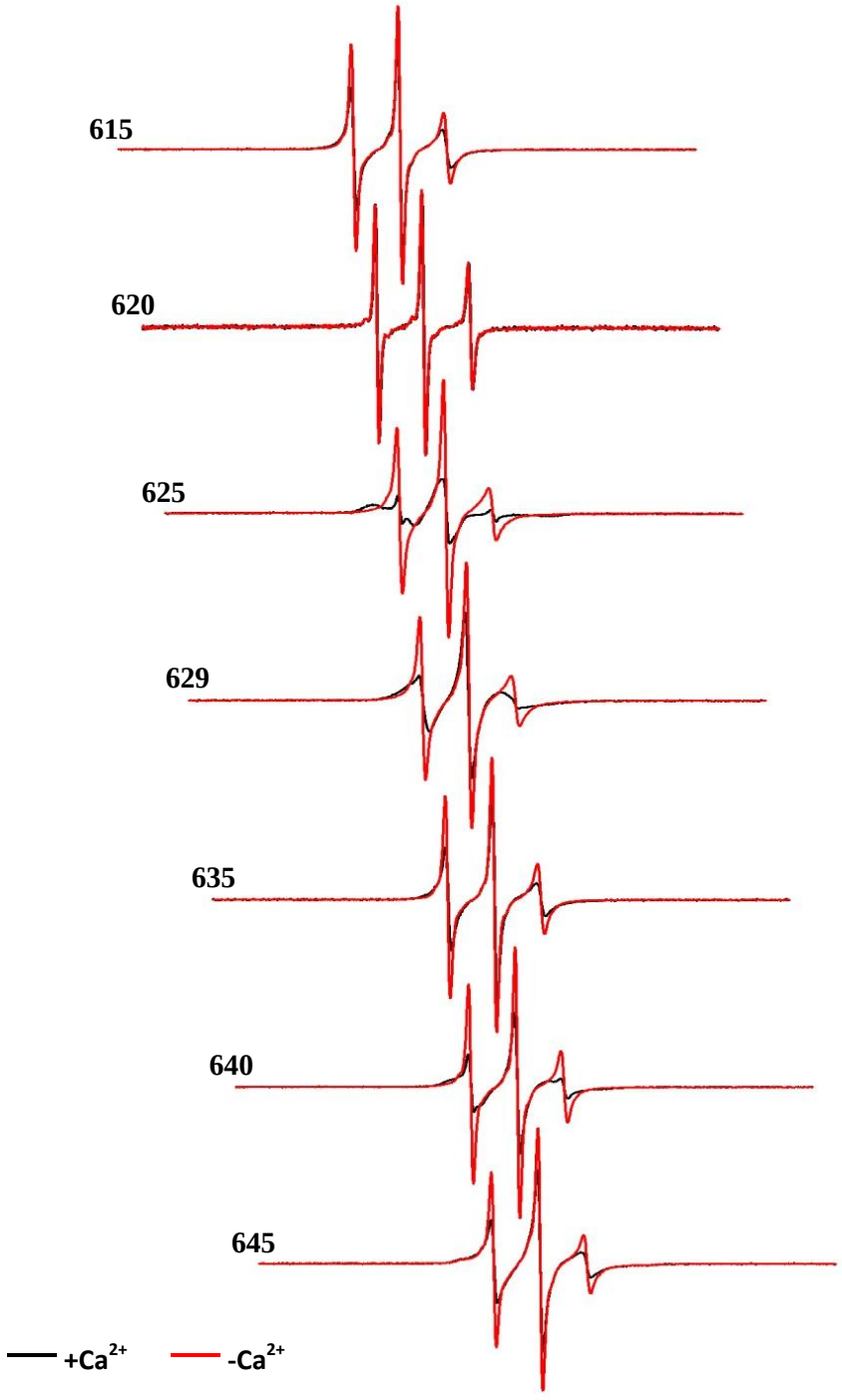

FIGURE 17. CW-EPR spectra of sites on the FG-loop of CBD2. The calcium-bound state is shown in black and the calcium-unbound is in red. Most of the spectra show a consistent pattern of decreased spin label motion when calcium ions are bound, as seen by the more rounded lineshapes. However, motion stays fairly fast.

Each construct with a mutation on the FG-loop was made as a double mutant with site 457 on CBD1 and site 557 on CBD2. All samples showed stable CW-EPR spectra with little to no change between calcium-bound and -unbound forms. Still, these samples show a similar pattern as the single mutants described above: spin label motion decreases when calcium ions are bound.

When most of these samples were analyzed with pulsed EPR, a similar, yet varied, pattern emerged (457-625 and 557-620 were not analyzed). Spectra and determined distance distributions for mutants with 457 can be seen in Figure 18 and those with 557 are in Figure 19. In double mutants from the helix to site 457 of CBD1, there was little change apparent in the results. Some samples, however, differed in signal-to-noise ratio between calcium-bound and -unbound samples. 457-635 simply had no apparent echo, even though the same sample gave very clean CW-EPR spectra. Alternatively, samples with site 557 often experienced a shift in population of distances. Constructs 557-615, 557-625, 557-640, and 557-645 experienced this effect. Other samples showed very little change or impact from the binding of calcium ions. As this occurred on a site- and binding state-dependent basis, it revealed some information about the movement (or lack thereof) of the FG-loop upon binding of calcium ions. In essence, this suggests that there is potentially some local conformational change as NCX1.1 carries out its function.

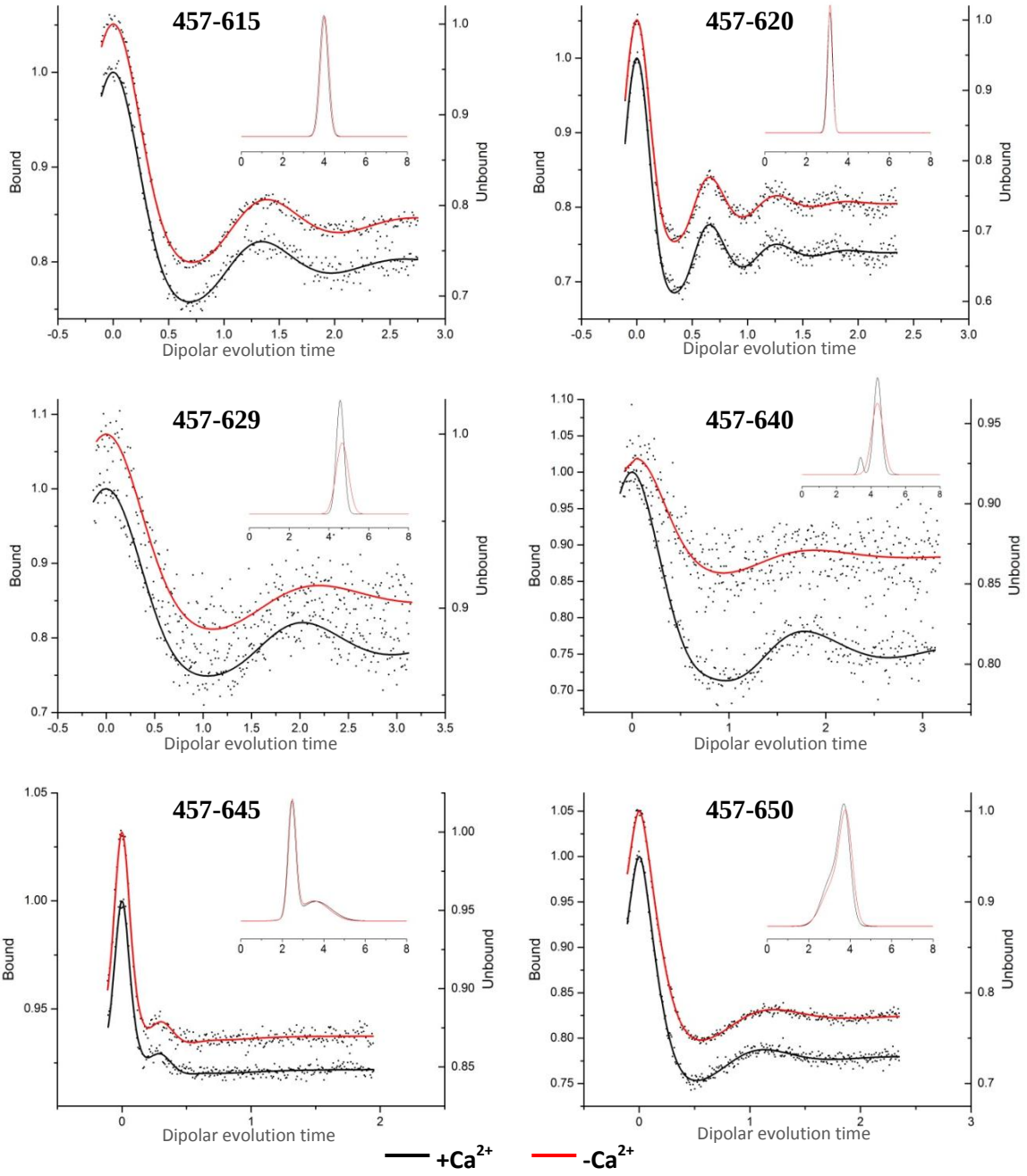

FIGURE 18. Pulsed EPR spectra of double mutants including sites on the FG-loop of CBD2 and site 457 of CBD1. Samples incubated with $CaCl_2$ are shown in black and those incubated with EDTA are shown in red. Y-axis for both calcium-bound and -unbound mark the time domain signal.

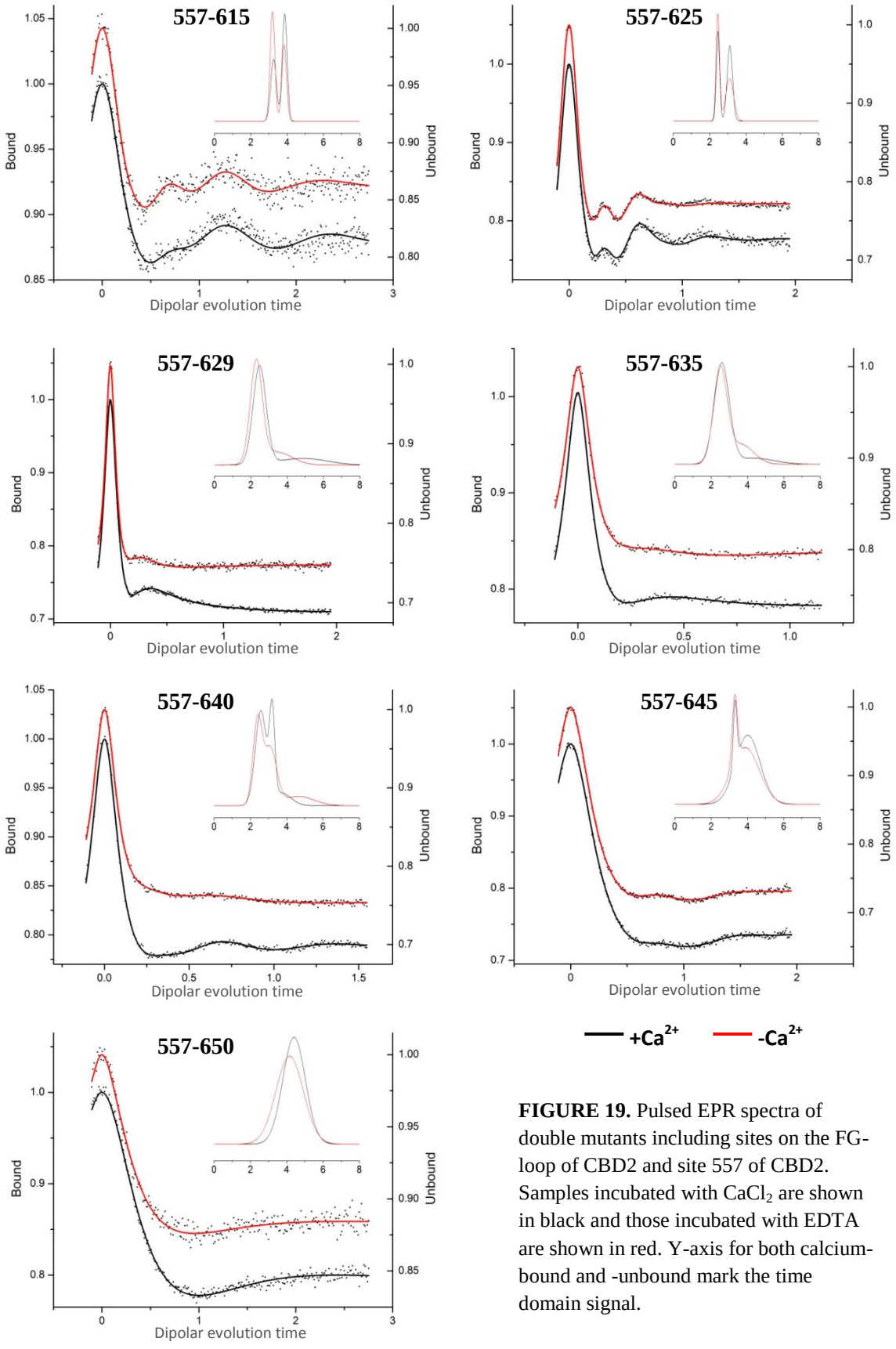

FIGURE 19. Pulsed EPR spectra of double mutants including sites on the FG-loop of CBD2 and site 557 of CBD2. Samples incubated with $CaCl_2$ are shown in black and those incubated with EDTA are shown in red. Y-axis for both calcium-bound and -unbound mark the time domain signal.

Discussion

Structural studies of NCX isoforms have focused on the ability of CBD1 and CBD2 to move relative to one another via the hinge region that connects them, but recent research with both NMR and EPR suggests that they likely stay stable in terms of their relative conformation. However, small elements of their structures may prove to be important for interactions within the protein and with other molecules. In the case of the cardiac exchanger NCX1.1, an extended loop region, called the FG-loop, and a nearby α-helix could be important for such interactions.

In the case of the helix, few, if any, studies have explored the properties and movements of the nine-residue α-helical region. Previously-determined structures have pinpointed the location of the helix as near the hinge region and calcium-binding region of CBD1. Because the α-helix sits adjacent to the FG-loop region, or potentially within the mobile unstructured loop, it could experience some movement upon calcium binding or other interactions that allow it to reach the CBD1 calcium-binding site. We showed that the helix stays intact whether calcium is bound or unbound. If it does have a role in the exchange mechanism of NCX1.1, this mechanism likely requires the helical conformation. Conversely, other distance measurements using pulsed EPR exhibited little movement of the α-helix relative to the CBDs. These results likely mean that there is not much movement of the helix upon binding of calcium ions. Any movement the helix experiences is likely a subtle "twist" and not a substantial change in position. This twist would leave site 659 in the same place and rotate around it, moving 667 just a few angstroms. It is also possible that the helix shifts it conformation slightly. Though low temperature CW-EPR spectra showed little conformational change in the α-helix, it is

inherently bent a small amount and could simply rotate this structure in some way, keeping intrahelical distances constant and slightly varying its location relative to both CBDs. Nonetheless, it is unlikely that any of these slight movements have an impact on the activity of NCX1.1 or the ability of the CBD1 binding sites to bind calcium ions.

As for the CBD2 FG-loop, it has been suggested both as a necessary piece of regulation (Villa-Abrille et al. 2008) and as unnecessary (Ottolia et al. 2009) for the exchange mechanism of NCX1.1. As previous research has not elucidated the structure of NCX1.1, it has been difficult to completely understand the arrangement and movement of the NCX1.1 FG-loop. Based on the structure of the NCX1.4 CBDs, it has been suspected that the FG-loop is extended out from CBD2. However, the FG-loop of NCX1.1 CBD2 is 35 residues longer than that of NCX1.4, so there could be significant differences between the two.

CW-EPR analysis reveals some insight into motions of the FG-loop. Single residues along the loop do go through a transition in motion from less restricted without calcium ions to more restricted with calcium bound. Some of the residues that are likely to be the farthest from CBD2 (625, 629, 640) show the most substantial changes in CW-EPR lineshape when calcium ions are bound. This could be due to an interaction with CBD1 or CBD2 at some region, though it is unclear where that interaction would take place. We suspect that there may be an interaction of the loop with the calcium-binding loops of CBD1, but again, there is no concrete evidence of that to this point. These analyses show that there is likely motion, though further research will be needed to determine more specificities of this motion.

Pulsed EPR was used to gain an understanding of where the FG-loop of CBD2 might be moving and what interactions it might have with either CBD. Spectra for double mutants with 457 (CBD1) show very little change in calculated distances, though 457-640 seems to have some difference between calcium-bound and -unbound states in the form of a second population at a shorter distance when calcium ions are bound. 457-629 is the only other standout, simply showing a broader distribution of possible distances in the calcium-unbound state. A sample of 457-635 was analyzed, but produced no signal. We suspect the distance between labels may be too great to see in the sample, though repeated experiments will have to be used to verify this supposition.

Double mutants that included site 557 on CBD2 showed significantly more population shifts or changes in the breadth of the distribution between calcium-bound and -unbound states. Constructs 557-615, 557-625, 557-640, and 557-645 show shifts in populations between states, though the latter two experience less than the former two. The other three samples resulted in spectra that vary in distance by a slight amount or change in breadth of the distribution peak. The non-sequential nature of these results seems to suggest a sort of bending of the FG-loop, with some regions experiencing more change than others.

With both the pulsed EPR and CW-EPR results, it seems that there is some change in movement of the FG-loop, though it is simply not clear what this motion entails. CW-EPR spectra show that the binding of calcium ions reduces the motion of the FG-loop in some way, though pulsed EPR results suggest that any change of the loop orientation relative to either CBD is minimal. While it is apparent that the binding of

calcium ions affects the FG-loop in some way, further research will be needed to firmly establish the details of this movement and its impact on the mechanism of NCX1.1.

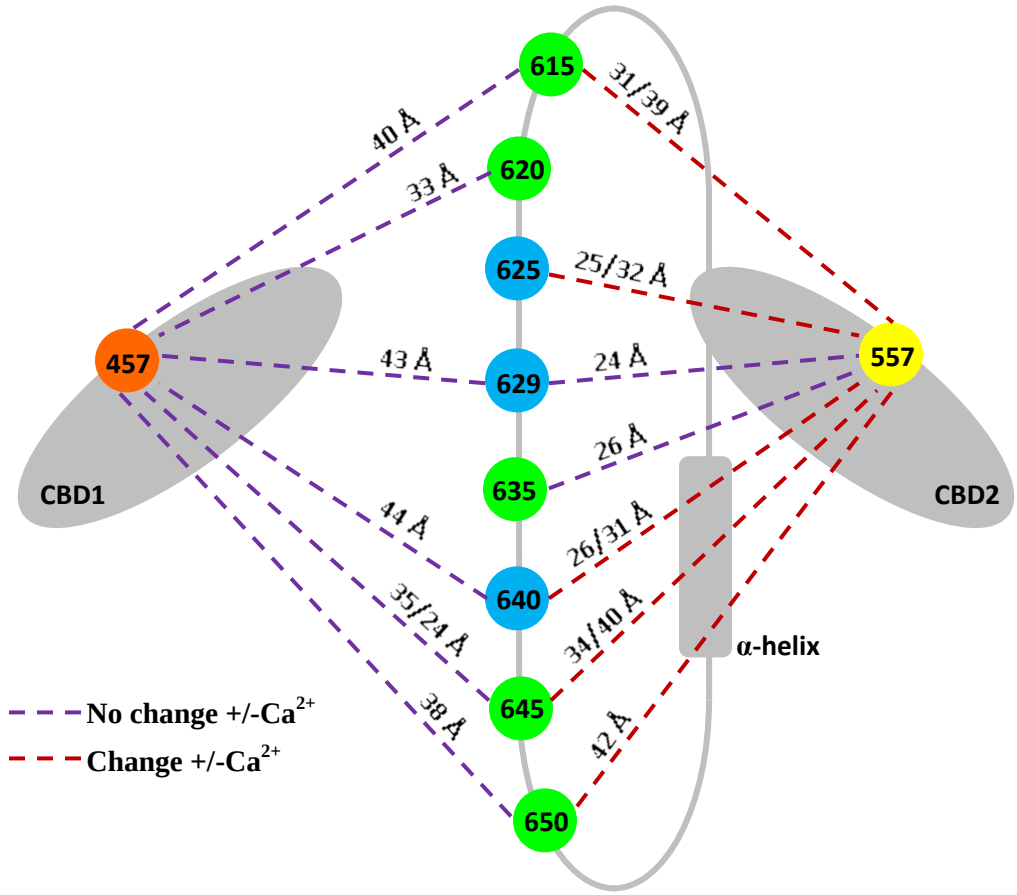

FIGURE 20. A diagram of the FG-loop residues and their relation to both CBD1 and CBD2 as analyzed with pulsed EPR. Each residue on the FG-loop is shown as a green circle, and those that showed the most significant changes in their CW-EPR spectra when calcium ions are bound are shown as cyan. 457 on CBD1 (orange circle) and 557 on CBD2 (yellow circle) were used in double mutants, and dashed lines connect these residues to FG-loop residues with calculated distances noted for each (two distances for two peaks). Distances with no change upon calcium binding are shown in purple and those with either a change in populations or slight changes in a single peak are shown in maroon.

Further Work

The data described above has provided a significant amount of information regarding the α-helix, FG-loop, and their motions relative to the CBDs of NCX1.1. However, further analysis of the movement of the FG-loop would be useful in understanding what motions are actually taking place. Double mutants with other sites on CBD1 and CBD2 could provide answers to this question. Also, investigating the interaction of the FG-loop to the XIP domain would provide a structural explanation of this interaction as well as elaborating on how the CBDs might orient relative to the long linkers that connect them to the transmembrane domain. These details would help to elaborate on the current structural model and fill in some gaps of the mechanistic details of ion transport by NCX1.1.

REFERENCES

Alberts, B., Johnson, A., Lewis, J., Raff, M., Roberts, K., and Walter, P. *Molecular Biology of the Cell, 5th Ed.* Garland Science: 2007.

Bassani, J.W.M., Bassani, R.A., and Bers, D.M. (1994) Relaxation in rabbit and rat cardiac cells: species-dependent differences in cellular mechanisms. *J. Physiol.* **476** (2), 279-293.

Bers, D.M. and Despa, S. (2006) Cardiac myocytes Ca^{2+} and Na^{+} regulation in normal and failing hearts. *J. Pharmacol. Sci.* **100** (5), 315-322.

Bers, D.M. and Ginsburg, K.S. (2007) Na:Ca stoichiometry and cytosolic Ca-dependent activation of NCX in intact cardiomyocytes. *Ann. N.Y. Acad. Sci.* **1099**, 326-338.

Breukels, V. and Vuister, G.W. (2010) Binding of calcium is sensed structurally and dynamically throughout the second calcium-binding domain of the sodium/calcium exchanger. *Proteins* **78** (8), 1813-1824.

Bridge, J.H., Spitzer, K.W., and Ershler, P.R. (1988) Relaxation of isolated ventricular cardiomyocytes by a voltage-dependent process. *Science* **241** (4867), 823-825.

Cai, X. and Lytton, J. (2004) The cation/Ca^{2+} exchanger superfamily: phylogenetic analysis and structural implications. *Mol. Biol. Evol.* **21** (9), 1692-1703.

Canzoniero, L.M., Rossi, A., Taglialatela, M., Amoroso, S., Annunziato, L., and Di Renzo, G. (1992) The Na^{+}-Ca^{2+} exchanger activity in cerebrocortical nerve endings is reduced in old compared to young and mature rats when it operates as a Ca^{2+} influx or efflux pathway. *Biochim. Biophys. Acta* **1107** (1), 175-178.

Chaptal, V., Ottolia, M., Mercado-Besserer, G., Nicoll, D.A., Philipson, K.D., and Abramson, J. (2009) Structure and functional analysis of a Ca^{2+} sensor mutant of the Na^{+}/Ca^{2+} exchanger. *J. Biol. Chem.* **284** (22), 14688-14692.

Chiang, Y.W., Borbat, P.P., and Freed, J.H. (2005) The determination of pair distance distributions by pulsed EPR using Tikhonov regularization. *J. Magn. Reson.* **172**b (2), 279-295.

Delbridge, L.M.D., Bassani J.W.M., and Bers, D.M. (1996) Steady-state twitch Ca^{2+} fluxes and cytosolic Ca^{2+} buffering in rabbit ventricular myocytes. *Am. J. Physiol. Cell Physiol.* **270** (1), C192-C199.

Despa, S., Islam, M.A., Weber, C.R., Pogwizd, S.M., and Bers, D.M. (2002) Intracellular Na^{+} concentration is elevated in heart failure but Na/K pump function is unchanged. *Circulation* **105** (21), 2543-2548.

Doyle, D.A., Cabral, J.M., Pfuetzner, R.A., Kuo, A., Gulbis, J.M., Cohen, S.L., Chait, B.T., and MacKinnon, R. (1998) The structure of the potassium channel: molecular basis of K^+ conduction and selectivity. *Science* **280** (5360), 69-77.

Dyck, C., Omelchenko, A., Elias, C.L., Quednau, B.D., Philipson, K.D., Hnatowich, M., and Hryshko, L.V. (1999) Ionic regulatory properties of brain and kidney splice variants of the Ncx1 Na^+-Ca^{2+} exchanger. *J. Gen. Physiol.* **114** (5), 701-711.

Elbaz, B., Alperovitch, A., Gottesman, M.M., Kimchi-Sarfaty, C., and Rahamimoff, H. (2008) Modulation of Na^+-Ca^{2+} exchanger expression by immunosuppressive drugs is isoform-specific. *Mole. Pharmacol.* **73** (4), 1254-1263.

Giladi, M., Boyman, L., Mikhasenko, H., Hiller, R., and Khananshvili, D. (2010) Essential role of the CBD1-CBD2 linker in slow dissociation of Ca^{2+} from the regulatory two-domain tandem of NCX1. *J. Biol. Chem.* **285** (36), 28117-28125.

Gomez-Villafuertes, R., Mellström, B., and Naranjo, J.R. (2007) Searching for a role of NCX/NCKX exchangers in neurodegeneration. *Mol. Neurobiol.* **35** (2), 195-202.

Gouaux, E. and MacKinnon, R. (2005) Principles of selective ion transport in channels and pumps. *Science* **310** (5753), 1461-1465.

Hilge, M., Aelen, J., Foarce, A., Perrakis, A., and Vuister, G.W. (2009) Ca^{2+} regulation in the Na^+/Ca^{2+} exchanger features a dual electrostatic switch mechanism. *Proc. Natl. Acad. Sci. U.S.A.* **106** (34), 14333-14338.

Hilge, M., Aelen, J., and Vuister, G.W. (2006) Ca^{2+} regulation in the Na^+/Ca^{2+} exchanger involves two markedly different Ca^{2+} sensors. *Mol. Cell* **22** (1), 15-25.

Hilge, M., Aelen, J., Perrakis, A., and Vuister, G.W. (2007) Structural basis for Ca^{2+} regulation in the Na^+/Ca^{2+} exchanger. *Ann. N.Y. Acad. Sci.* **1099**, 7-15.

Hilgemann, D.W. (1990) Regulation and deregulation of cardiac Na^+-Ca^{2+} exchange in giant excised sarcolemmal membrane patches. *Nature* **344** (6364), 242-245.

Hill, R.W., Wyse, G.A., and Anderson, M. *Animal Physiology, 2nd Ed.* Sinauer Associates, Inc.: 2008.

Hübner, C.A. and Jentsch, T.J. (2002) Ion channel diseases. *Hum. Mol. Genet.* **11** (20), 2435-2445.

Hurtado, C., Prociuk, M., Maddaford, T.G., Dibrov, E., Mesaeli, N., Hryshko, L.V., and Pierce, G.N. (2006) Cells expressing unique Na^+/Ca^{2+} exchange (NCX1) splice variants exhibit different susceptibilities to Ca^{2+} overload. *Am. J. Physiol. Heart Circ. Physiol.* **290** (5), H2155-H2162.

Hustedt, E.J., Stein, R.A., Sethaphong, L., Brandon, S., Zhou, Z., and Desensi, S.C. (2006) Dipolar coupling between nitroxide spin labels: the development and application of a tether-in-a-cone model. *Biophys. J.* **90** (1), 340-356.

John, S.A., Ribalet, B., Weiss, J.N., Philipson, K.D., and Ottolia, M. (2011) Ca^{2+}-dependent structural rearrangements within Na^{+}-Ca^{2+} exchanger dimers. *Proc. Natl. Acad. Sci. U. S. A.* **108** (4), 1699-1704.

Johnson, E., Bruschweiler-Li, L., Showalter, S.A., Vuister, G.W., Zhang, F., and Brüschweiler, R. (2008) Structure and dynamics of Ca^{2+}-binding domain 1 of the Na^{+}/Ca^{2+} exchanger in the presence and in the absence of Ca^{2+}. *J. Mol. Biol.* **377** (3), 945-955.

Jorgensen, P.L., Håkansson, K.O., and Karlish, S.J.D. (2003) Structure and mechanism of Na,K-ATPase: functional sites and their interactions. *Ann. Rev. Physiol.* **65**, 817-849.

Klug, C.S. and Feix, J.B. (2008) Methods and applications of site-directed spin labeling EPR spectroscopy. *Methods Cell Biol.* **84**, 617-658.

Kohlhaas, M. and Maack, C. (2010) Adverse bioenergetic consequences of Na^{+}-Ca^{2+} exchanger-mediated Ca^{2+} influx in cardiac myocytes. *Circulation* **122** (22), 2273-2280.

Laemmli, U.K. (1970) Cleavage of structural proteins during the assembly of the head of bacteriophage T4. *Nature* **227** (5259), 680-685.

Li, Z., Nicoll, D.A., Collins, A., Hilgemann, D.W., Filoteo, A.G., Penniston, J.T., Weiss, J.N., Tomich, J.M., and Philipson, K.D. (1991) Identification of a peptide inhibitor of the cardiac sarcolemmal Na^{+}-Ca^{2+} exchanger. *J. Biol. Chem.* **266** (2), 1014-1020.

Li, Z., Matsuoka, S., Hryshko, L.V., Nicoll, D.A., Bersohn, M.M., Burke, E.P., Lifton, R.P., and Philipson, K.D. (1994) Cloning of the NCX2 isoform of the plasma membrane Na^{+}-Ca^{2+} exchanger. *J. Biol. Chem.* **269** (26), 17434-17439.

López-López, J.R., Shacklock, P.S., Balke, C.W., Wier, W.G. (1995) Local calcium transients triggered by single L-type calcium channel currents in cardiac cells. *Science* **268** (5213), 1042-1045.

Louch, W.E., Hougen, K., Mork, H.K., Swift, F., Aronsen, J.M., Sjaastad, I., Reims, H.M., Roald, B., Andersson, K.B., Christensen, G., and Sejersted, O.M. (2010) Sodium accumulation promotes diastolic dysfunction in end-stage heart failure following *Serca2* knockout. *J. Physiol.* **588** (3), 465-478.

Lytton, J. (2007) Na^{+}/Ca^{2+} exchangers: three mammalian gene families control Ca^{2+} transport. *Biochem. J.* **406** (3), 365-382.

Maack, C., Ganesan, A., Sidor, A., and O'Rourke, B. (2005) Cardiac sodium-calcium exchanger is regulated by allosteric calcium and exchanger inhibitory peptide at distinct sites. *Circ. Res.* **96** (1), 91-99.

Martinez, Y. and N'Gouemo, P. (2010) Blockade of the sodium calcium exchanger exhibits anticonvulsant activity on a pilocarpine model of acute seizures in rats. *Brain Res.* **17** (1366), 211-216.

Matsuoka, S. and Hilgemann, D.W. (1992) Steady-state and dynamic properties of cardiac sodium-calcium exchange. Ion and voltage dependence of the transport cycle. *J. Gen. Physiol.* **100** (6), 963-1001.

Mattson, M.P. and Chan, S.L. (2003) Neuronal and glial calcium signaling in Alzheimer's disease. *Cell Calcium* **34** (4-5), 385-397.

Michaelis, M.L., Johe, K., and Kitos, T.E. (1992) Age-dependent alterations in synaptic membrane systems for Ca^{2+} regulation. *Mech. Ageing Dev.* **25** (1-2), 215-225.

Milberg, P., Pott, C., Fink, M., Frommeyer, G., Matsuda, T., Baba, A., Osada, N., Breithardt, G., Noble, D., and Echardt, L. (2008) Inhibition of the Na^{+}/Ca^{2+} exchanger suppresses torsades de pointes in an intact heart model of long QT syndrome-2 and long QT syndrome-3. *Heart Rhythm* **5** (10), 1444-1452.

Mima, M., Kawai, C., Paku, K., Tomoo, K., Ishida, T., Sugiyama, S., Matsumura, H., Kitatani, T., Yoshikawa, H.Y., Maki, S., Adachi, H., Takano, K., Murakami, S., Inoue, T., More, Y., Kita, S., and Iwamoto, T. (2008) Crystallization and preliminary x-ray crystallographic analysis of Ca^{2+}-free primary Ca^{2+}-sensor of Na^{+}/Ca^{2+} exchanger. *Acta Cryst.* **64** (12), 1125-1127.

Morimoto, S. (2007) Sarcomeric proteins and inherited cardiomyopathies. *Cardiovasc. Res.* **77** (4), 659-666.

Nelson, D.L. and Cox, M.M. *Lehninger Principles of Biochemistry, 4th Ed.* W.H. Freeman: 2004.

Nicoll, D.A., Longoni, S., and Philipson, K.D. (1990) Molecular cloning and functional expression of the cardiac sarcolemmal Na^{+}-Ca^{2+} exchanger. *Science* **250** (4980), 562-565.

Nicoll, D.A., Hryshko, L.V., Matsuoka, S., Frank, J.S., and Philipson, K.D. (1996) Mutation of amino acid residues in the putative transmembrane segments of the cardiac sarcolemmal Na^{+}-Ca^{2+} exchanger. *J. Biol. Chem.* **271** (23), 13385-13391.

Nicoll, D.A., Quednau, B.D., Qui, Z., Xia, Y.-R., Lusis, A.J., and Philipson, K.D. (1996) Cloning of a third mammalian Na^{+}-Ca^{2+} exchanger, NCX3. *J. Biol. Chem.* **271** (40), 24914-24921.

Nicoll, D.A., Ottolia, M., Lu, L., Lu, Y., and Philipson, K.D. (1999) A new topological model of the cardiac sarcolemmal Na^{+}-Ca^{2+} exchanger. *J. Biol. Chem.* **274** (2), 910-917.

Nicoll, D.A., Sawaya, M.R., Kwon, S., Cascio, D., Philipson, K.D., and Abramson, J. (2006) The crystal structure of the primary Ca^{2+} sensor of the Na^{+}/Ca^{2+} exchanger reveals a novel Ca^{2+} binding motif. *J. Biol. Chem.* **281** (31), 21577-21581.

Ottolia, M., Nicoll, D.A., and Philipson, K.D. (2009) Roles of two Ca^{2+}-binding domains in regulation of the cardiac Na^{+}-Ca^{2+} exchanger. *J. Biol. Chem.* **284** (47), 32735-32741.

Periasamy, M. and Huke, S. (2001) SERCA pump level is a critical determinant of Ca^{2+} homeostasis and cardiac contractility. *J. Mol. Cell Cardiol.* **33** (6), 1053-1063.

Pieske, B., Maier, L.S., Piacentino, V. 3rd, Weisser, J., Hasenfuss, G., and Houser, S. (2002) Rate dependence of $[Na^{+}]i$ and contractility in nonfailing and failing human myocardium. *Circulation* **106** (4), 447-453.

Quednau, B.D., Nicoll, D.A., and Philipson, K.D. (1997) Tissue specificity and alternative splicing of the Na^{+}/Ca^{2+} exchanger isoforms NCX1, NCX2, and NCX3 in rat. *Am. J. Physiol. Cell Physiol.* **272** (4), C1250-C1261.

Quednau, B.D., Nicoll, D.A., and Philipson, K.D. (2004) The sodium/calcium exchanger family – SLC8. *Pflug. Arch. Eur. J. Physiol.* **447** (5), 543-548.

Rabenstein, M.D. and Shin, Y.K. (1995) Determination of the distance between two spin labels attached to a macromolecule. *Proc. Natl. Acad. Sci. U.S.A.* **92** (18), 8239-8243.

Radwański, P.B. and Poelzing, S. (2011) NCX is an important determinant for premature ventricular activity in a drug-induced model of Andersen-Tawil syndrome. *Cardiovasc. Res.* **92** (1), 57-66.

Reeves, J.P., Condrescu, M., Chernaya, G., and Gardner, J.P. (1994) Na^{+}/Ca^{2+} antiport in the mammalian heart. *J. Exp. Biol.* **196** (1), 375-388.

Reeves, J.P. and Condrescu, M. (2003) Allosteric activation of sodium-calcium exchange activity by calcium: persistence at low calcium concentrations. *J. Gen. Physiol.* **122** (5), 621-639.

Reeves, J.P. and Condrescu, M. (2008) Ionic regulation of the cardiac sodium-calcium exchanger. *Channels* **2** (5), 322-328.

Ren, X., Nicoll, D.A., Galang, G., and Philipson, K.D. (2008) Intermolecular cross-linking of Na^{+}-Ca^{2+} exchanger proteins: evidence for dimer formation. *Biochemistry* **47** (22), 6081-6087.

Saito, R. Kaneko, E., Tanaka, Y., Honda, K., Matsuda, T., Baba, A., Komuro, I., Kita, S., Iwamoto, T., and Takano, Y. (2009) Involvement of Na^{+}/Ca^{2+} exchanger pentylenetetrazol-induced convulsion by use of Na^{+}/Ca^{2+} exchanger knockout mice. *Biol. Pharm. Bull.* **32** (11), 1928-1930.

Salinas, R.K., Bruschweiler-Li, L., Johnson, E., and Brüschweiler, R. (2011) Ca^{2+} binding alters the interdomain flexibility between the two cytoplasmic calcium-binding domains in the Na^{+}/Ca^{2+} exchanger. *J. Biol. Chem.* **286** (37), 32123-32131.

Schwarz, E.M. and Benzer, S. (1997) Calx, a Na-Ca exchanger gene of Drosophila melanogaster. *Proc. Natl. Acad. Sci.* **94** (19), 10249-10254.

Sokolow, S., Luu, S.H., Headley, A.J., Hanson, A.Y., Kim, T., Miller, C.A., Vinters, H.V., Gylys, K.H. (2011) High levels of synaptosomal Na^{+}-Ca^{2+} exchangers (NCX1, NCX2, NCX3) co-localized with amyloid-beta in human cerebral cortex affected by Alzheimer's disease. *Cell Calcium* **49** (4), 208-216.

Steinhoff, H-J. (2002) Methods for study of protein dynamics and protein-protein interaction in protein-ubiquitination by electron paramagnetic resonance spectroscopy. *Front. Biosci.* **7**, c97-c110.

Sunandana, C.S. (1998) Techniques and applications of electron spin resonance. *Bull. Mater. Sci.* **21** (1), 1-70.

Villa-Abrille, M.C., Sidor, A., and O'Rourke, B. (2008) Insulin effects on cardiac Na^{+}/Ca^{2+} exchanger activity. *J. Biol. Chem.* **283** (24), 16505-16513.

Wei, S., Ruknudin, A.M., Shou, M., McCurley, J.M., Hanlon, S.U., Elgin, E., Schulze, D.H., and Haigney, M.C.P. (2007) Muscarinic modulation of the sodium-calcium exchanger in heart failure. *Circulation* **115** (10), 1225-1233.

Weil, J.A., Bolton, J.R., and Wertz, J.E. *Electron Paramagnetic Resonance: Elementary Theory and Practical Applications*. John Wiley & Sons, Inc.: 1994.

Wu, A., Derrico, C.A., Hatem, L., and Colvin, R.A. (1997) Alzheimer's amyloid-beta peptide inhibits sodium/calcium exchange measured in rat and human brain plasma membrane vesicles. *Neuroscience* **80** (3) 675-684.

Wu, M., Wang, M., Nix, J., Hryshko, L.V., and Zheng, L. (2009) Crystal structure of CBD2 from the *Drosophila* Na^{+}/Ca^{2+} exchanger: diversity of Ca^{2+} regulation and its alternative splicing modification. *J. Mol. Biol.* **387** (1), 104-112.

Wu, M., Le, H.D., Wang, M., Yurkov, V., Omelchenko, A., Hnatowich, M., Nix, J., Hryshko, L.V., and Zheng, L. (2010) Crystal structures of progressive Ca^{2+} binding states of the Ca^{2+} sensor Ca^{2+} binding domain 1 (CBD1) from the CALX Na^{+}/Ca^{2+} exchanger reveal incremental conformational transitions. *J. Biol Chem.* **385** (4), 2554-2561.